

AD _____

CONTRACT NUMBER DAMD17-93-C-3118

TITLE: Three-Dimensional Structure Determination of Botulinum Toxin

PRINCIPAL INVESTIGATOR: Ray C. Stevens, Ph.D.

CONTRACTING ORGANIZATION: University of California
Riverside, California 92521

REPORT DATE: July 1998

19981029014

TYPE OF REPORT: Annual

PREPARED FOR: U.S. Army Medical Research and Materiel Command
Fort Detrick, Maryland 21702-5012

DISTRIBUTION STATEMENT: Approved for public release;
distribution unlimited

The views, opinions and/or findings contained in this report are those of the author(s) and should not be construed as an official Department of the Army position, policy or decision unless so designated by other documentation.

REPORT DOCUMENTATION PAGE

*Form Approved
OMB No. 0704-0188*

Public reporting burden for this collection of information is estimated to average 1 hour per response, including the time for reviewing instructions, searching existing data sources, gathering and maintaining the data needed, and completing and reviewing the collection of information. Send comments regarding this burden estimate or any other aspect of this collection of information, including suggestions for reducing this burden, to Washington Headquarters Services, Directorate for Information Operations and Reports, 1215 Jefferson Davis Highway, Suite 1204, Arlington, VA 22202-4302, and to the Office of Management and Budget, Paperwork Reduction Project (0704-0188), Washington, DC 20503.

1. AGENCY USE ONLY <i>(Leave blank)</i>	2. REPORT DATE July 1998	3. REPORT TYPE AND DATES COVERED Annual (1 Aug 97 - 30 Jun 98)	
4. TITLE AND SUBTITLE Three-Dimensional Structure Determination of Botulinum Toxin		5. FUNDING NUMBERS DAMD17-93-C-3118	
6. AUTHOR(S) Stevens, Ray C., Ph.D.			
7. PERFORMING ORGANIZATION NAME(S) AND ADDRESS(ES) University of California Riverside, California 92521		8. PERFORMING ORGANIZATION REPORT NUMBER	
9. SPONSORING / MONITORING AGENCY NAME(S) AND ADDRESS(ES) U.S. Army Medical Research and Materiel Command Fort Detrick, Maryland 21702-5012		10. SPONSORING / MONITORING AGENCY REPORT NUMBER	
11. SUPPLEMENTARY NOTES			
12a. DISTRIBUTION / AVAILABILITY STATEMENT Approved for public release; distribution unlimited		12b. DISTRIBUTION CODE	
13. ABSTRACT <i>(Maximum 200 words)</i> The immediate goals of the contract on the structure and function relationship of botulinum neurotoxin are: 1) Determine the three-dimensional structure of botulinum neurotoxin at atomic resolution by x-ray crystallography. 2) Based on the structure of the neurotoxin, understand the toxins mechanism of action. We have accomplished the first goal of determining the three-dimensional structure of the 150 kD botulinum neurotoxin serotype A. The toxin is Y-shaped, with a very long alpha-helical translocation domain forming the backbone of the structure. The translocation domain is composed almost entirely of helices, 2 of which are 95 Å in length and form a pseudo-coiled coil. The binding domain and catalytic domain are more globular in shape, located at two different ends of the translocation domain. The overall dimensions of the protein are 120 Å x 80 Å x 40 Å. A complete description of the three-dimensional structure is described in the report (the manuscript will be published in the September issue of <i>Nature Structural Biology</i>). We have recently collected data on an inhibitor complex and a receptor complex. Refinement and analysis of the toxin with bound molecules will be completed within the next 12 months.			
14. SUBJECT TERMS 3-D structure, botulinum neurotoxin, inhibitor design, x-ray crystallography		15. NUMBER OF PAGES 60	
		16. PRICE CODE	
17. SECURITY CLASSIFICATION OF REPORT Unclassified	18. SECURITY CLASSIFICATION OF THIS PAGE Unclassified	19. SECURITY CLASSIFICATION OF ABSTRACT Unclassified	20. LIMITATION OF ABSTRACT Unlimited

FOREWORD

Opinions, interpretations, conclusions and recommendations are those of the author and are not necessarily endorsed by the U.S. Army.

Where copyrighted material is quoted, permission has been obtained to use such material.

Where material from documents designated for limited distribution is quoted, permission has been obtained to use the material.

RS Citations of commercial organizations and trade names in this report do not constitute an official Department of Army endorsement or approval of the products or services of these organizations.

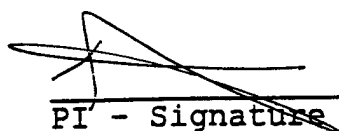
In conducting research using animals, the investigator(s) adhered to the "Guide for the Care and Use of Laboratory Animals," prepared by the Committee on Care and Use of Laboratory Animals of the Institute of Laboratory Resources, National Research Council (NIH Publication No. 86-23, Revised 1985).

For the protection of human subjects, the investigator(s) adhered to policies of applicable Federal Law 45 CFR 46.

RS In conducting research utilizing recombinant DNA technology, the investigator(s) adhered to current guidelines promulgated by the National Institutes of Health.

RS In the conduct of research utilizing recombinant DNA, the investigator(s) adhered to the NIH Guidelines for Research Involving Recombinant DNA Molecules.

RS In the conduct of research involving hazardous organisms, the investigator(s) adhered to the CDC-NIH Guide for Biosafety in Microbiological and Biomedical Laboratories.



PI - Signature

7/29/98
Date

Three-Dimensional Structure Determination of Botulinum Toxin
Contract: DAMD17-93-C-3118

TABLE OF CONTENTS

FRONT COVER	i
SF 298 - Report Documentation page	ii
FOREWORD	iii
INTRODUCTION	
Nature of Problem	1
Background of Previous Work	2
Purpose of Present Work	2
Methods of Approach	2
BODY	
Experimental Methods	4
Relationship to Goals of Research	7
CONCLUSION	8
BIBLIOGRAPHY (Manuscripts, Meetings, Personnel)	11
APPENDIX	
F. Chen, G. Kuziemko, P. Amersdorfer, C. Wong, J.D. Marks, R.C. Stevens "Antibody Mapping to Domains of Botulinum Neurotoxin serotype A in the Complexed and Uncomplexed Forms" <i>Infection & Immunity</i> 65, 1626 (1997).	A1
R. Burkhard, F. Chen, G. Kuziemko, R.C. Stevens "Electron Density Projection Maps of the 900 kD Botulinum Neurotoxin Complex by Electron Crystallography" <i>J. Structural Biology</i> 120, 78 (1997).	B1

19981029 014

- D.B. Lacy and R.C. Stevens "Recombinant Expression and Purification of the Botulinum Neurotoxin A Translocation Domain", *Protein Expression and Purification* **11**, 195 (1997). C1
- F. Chen, G. M. Kuziemko, R.C. Stevens "Biophysical Characterization of the Stability of the 150-Kilodalton Botulinum Toxin, the Non-toxic Component, and the 900-Kilodalton Botulinum Toxin Complex Species" *Infection & Immunity* **66**, 2420 (1998). D1
- B. Lacy, W. Tepp, B. DasGupta, R.C. Stevens "Three-dimensional Crystal Structure of Botulinum Neurotoxin and Implications in Toxicity" in press *Nature Structural Biology* (1998). E1

INTRODUCTION

Nature of Problem

To determine the 3-dimensional structure of botulinum neurotoxins and their isolated domains. Priority of the specifications are determined in consultation with the Contracting Officer's Representative (COR). The following specifications are listed in the contract section C - Statement of Work:

- 1) Crystallization of the 150 kD holo-botulinum neurotoxin, serotype A, B, E.
- 2) Determination of the 3-dimensional structure of serotype A.
- 3) Given the structure of serotype A, the technique of molecular replacement will be used to determine the structure of serotype B and E.
- 4) Crystallization of Heavy chain neurotoxin serotype A.
- 5) Determination of the 3-dimensional structure of the isolated heavy chain. Molecular replacement using the structure of the intact holo-neurotoxin if the structure has not changed substantially. If not, isomorphous replacement will be used.
- 6) Crystallization of Light chain neurotoxin serotype A.
- 7) Determination of the 3-dimensional structure of the isolated light chain. Molecular replacement using the structure of the intact holo-neurotoxin if the structure has not changed substantially. If not, isomorphous replacement will be used.
- 8) Similar studies on other serotypes.

Based on the consultation with the COR, priority is to the 3-dimensional crystal structure of the 150 kD holo-botulinum neurotoxin serotype A (Item 2).

Background of Previous Work

Before funding of the contracted work for the structure determination of botulinum neurotoxin serotype A, we determined crystallization conditions of botulinum neurotoxin serotype A (Stevens et al, *J. Mol. Biol.* 222, 877 (1991)) and found the most suitable crystal form of serotype A for X-ray analysis are bipyramidal shaped crystals that crystallize in the hexagonal space group P3₁21 (or P3₂21) with one monomer per asymmetric unit. The unit cell dimensions are $a = b = 170.5 \text{ \AA}$, $c = 161.7 \text{ \AA}$. Native and derivative data sets have been collected in house (Room 405 Stanley Hall) at the University of California, Berkeley using a shared (with 3 other research groups) Rigaku RU-200 rotating anode generator and R-axis Image Plate area detector system.

During the first years of the contract, we reported that we had worked out the conditions to further purify the protein (isoelectric focusing and aggregation), stabilize the protein (zinc acetate, proteolytic inhibitors, ganglioside), and improve the crystal quality of the neurotoxin protein. We very carefully worked out condition to collect complete, accurate, and non-deteriorating x-ray diffraction data use flash freezing techniques to freeze the protein crystals at -170°C during x-ray irradiation. We collected a large amount of both native (7 sets) and heavy atom derivative data (20 sets) that is used to phase the x-ray diffraction pattern to yield the 3-dimensional structure of the neurotoxin. Data have been collected at the Brookhaven NSLS and Stanford SSRL synchrotron radiation facilities. We have collected data on serotype B and E and molecular replacement solutions are in progress (completion of Contract Goal C2).

Purpose of Present Work

We have completed the primary goal of the contract, the three-dimensional structure determination of botulinum neurotoxin. This work will appear in the September issue of *Nature Structural Biology*. We have collected data on serotype E at 2.8 Å resolution. We have also collected data of the toxin with catalytic site inhibitor, and data with the receptor Gt1b bound to the binding domain.

Methods of Approach

Using the technique of multiple isomorphous replacement, the 3-dimensional structure of botulinum neurotoxin was solved using diffraction data from native and heavy atom derivative data sets that are collected in house or at synchrotron facilities. The technique requires one to:

1) Bind heavy atoms to derivative the protein crystal and locate the position of the heavy atom using Patterson methods. The derivitized protein crystals must be isomorphous with the native protein crystals (except for the heavy atom itself) for the information to be interpretable.

2) Once the position of the heavy atoms were located, approximate phases can be calculated to allow one to observe the electron density of the protein molecule. The

program MLPHARE from the CCP4 program suite (CCP4, 1979, The SERC (UK) Collaborative Computing Project No. 4, a Suite of Programs for Protein Crystallography, distributed from Daresbury Laboratory, Warrington, WA4 4AD, UK) will be used to combine and phase heavy atom derivative data. All computations will be conducted on a Silicon Graphics INDIGO graphics workstation.

3) Fitting of electron density was made on a Silicon Graphics INDIGO graphics workstation using the program O (version 6.1; Alwyn Jones, 1997).

4) Upon completion of fitting the electron density, the experimental model was refined using the program XPLOR (version 3.851; Brunger, 1997) installed on a Silicon Graphics INDIGO graphics workstation.

An alternative to isomorphous replacement is the method of molecular replacement which depends on the presence of related structures in different crystals. Proteins which are homologous and have closely similar structures are particularly useful. The near identity of the structures implies relations between different structure amplitudes and phases which are helpful in solving phase problems. Serotypes A, B and E are similar as well as dissimilar (pharmacologically similar, antigenically different). Hence, once a structure is obtained for one serotype, the analysis of crystals of other serotypes can be aided by the molecular replacement technique. This is based on the assumption that the overall tertiary structure of all three serotypes are similar. If this is not the case, then a search for heavy atom derivatives will have to be conducted for all three serotypes.

The use of molecular replacement is being used with the inhibitor and receptor bound structures.

BODY - Experimental Methods

1. Structure Determination

Crystals were grown as described previously, but with a modified mother liquor of 150 mM magnesium acetate, 11% PEG 4000, and 100 mM tris-HCl pH 7. The crystals contain one monomer per asymmetric unit and are in spacegroup P3121 ($a = b = 170.5 \text{ \AA}$, $c = 161.1 \text{ \AA}$) with a solvent content of 70%. Derivatives were prepared by soaking crystals in: 1mM potassium tetrachloroaurate for 8-12 hrs, 1mM mercurous acetate for 6 hrs, 3mM methyl mercuric chloride for 6 hrs, 50mM samarium acetate for 12 hrs, or 0.5mM uranyl acetate for 6-10 hrs. Diffraction data for native and derivatized crystals were collected at 4 °C at SSRL, beamline 7-1 and beamline 9-1, at 1.08 Å and 0.98 Å, respectively. Crystals diffracted reasonably well for about 5 images using 1° oscillations before showing signs of radiation damage. Taking advantage of the high symmetry and the ability to translate bar shaped crystals allowed for complete data sets to be collected from a few crystals. All data were processed with DENZO and SCALEPACK, allowing for decreased resolution and increased mosaicity as the crystal decayed. The CCP4 suite of programs was used for scaling the data sets and locating the heavy atom positions. Patterson maps were viewed with XCONTUR. MLPHARE was used for heavy-atom position refinement and phase calculation. Phases were extended to 3.6 Å and improved by solvent flattening and histogram matching using the program DM³⁰. The model was built to 3.6 Å resolution using the program O³¹, and then, as more data was collected, extended to 3.2 Å. Maps were improved with phase combination using SIGMAA. Cycles of rebuilding, positional refinement, and simulated annealing using X-PLOR were continued until convergence. Excellent electron density exists throughout the model and 99% of the amino acids were visible. Not surprisingly, the two ill-defined regions of the structure are the site of proteolytic cleavage between the two chains and in a surface loop immediately following His560 of the translocation domain. Although botulinum neurotoxin serotype A crystallizes quite easily, the ability to collect x-ray diffraction data on protein crystals that are all "locked" into the same structure inside the crystal has become a hurdle in our efforts to determine the 3-dimensional structure. In layman's terms, botulinum neurotoxin molecules have the ability to conform to several different conformational structures caused by "floppy" or disordered regions of protein structure. This problem makes it difficult to merge together native data sets as well as heavy atom derivative data sets. This problem makes it difficult to use the techniques of isomorphous replacement with heavy atom derivatives since one data set is not similar enough to the next. To avoid this problem we have taken several different measures that are described below. These approaches have proven successful to other researchers that have encountered this problem. The problem of non-isomorphism is not uncommon in crystal structure determinations, particularly for neurotoxins (i.e. crystal structure determinations for cholera toxin, diphtheria toxin, pertussis toxin).

Table 1 Structure determination statistics**Diffraction data statistics**

Crystal	Resolution(Å)	Total obs.	Unique refl.	Completeness ¹ (%)	R _{merge} ² (%)
Native	20-3.2	172,169	40,110	98.2(94.3)	11.1(48.3)
CH ₃ HgCl	15-4.5	87,457	15,830	97.2(96.0)	10.7(27.7)
Hg ₂ (Ac) ₂	15-4.2	86,260	19,650	97.8(94.3)	9.1(24.5)
SmAc	15-4.5	22,797	12,516	78.5(78.2)	7.6(17.4)
UAc	15-4.5	22,795	11,796	71.9(73.6)	7.8(22.5)
KAuCl ₄	15-6.0	19,894	6,080	93.7(95.5)	9.4(18.2)

Phasing statistics

Derivative	Number of sites ³	Isomorphous R-factor ⁴ (%)	Phasing power ⁵ Cent.	Phasing power ⁵ Acent.	R _{Cullis} ⁶ Cent.	R _{Cullis} ⁶ Acent.
CH ₃ HgCl	6	21.7	1.03	1.64	0.68	0.65
Hg ₂ (Ac) ₂	6	21.0	0.96	1.36	0.76	0.76
SmAc	3	14.9	0.77	1.07	0.83	0.87
UAc	3	15.2	0.66	1.04	0.88	0.91
KAuCl ₄	1	15.2	0.63	1.03	0.88	0.88
FOM before solvent flattening		0.48				
FOM after solvent flattening		0.74				

Refinement statistics

R-factor/Free R	20.0/27.9
R.m.s.d. bond lengths	0.008 Å
R.m.s.d. bond angles	1.5 degrees

¹Numbers in parentheses indicate statistics for highest resolution shells.

²R_{merge} = $S_h S_i |I_{hi} - \langle I_{hi} \rangle| / S_h S_i |I_{hi}|$, where h specifies unique indices, i indicates symmetry equivalent observations of h , and $\langle I_{hi} \rangle$ is the mean value.

³The mercury and gold derivatives shared overlapping sites. Similarly, the samarium and uranyl derivatives shared sites. However, the different occupancies yielded enough new phase information to improve the quality of the maps.

⁴The isomorphous R factor = $S_h ||F_{PH}|| - ||F_p|| / S_h ||F_p||$, where $|F_{PH}|$ and $|F_p|$ are the measured structure factor amplitudes of the derivative and native structures.

⁵Phasing power is the mean value of the heavy atom structure factor amplitude divided by the residual lack of closure error.

⁶R_{Cullis} is the mean residual lack of closure error divided by the isomorphous difference.

2. Proteolytic Assay of Catalytic Domain

Because of the need for a means to evaluate the quality of protein used in crystal growth experiments in addition to the fact that we need to learn as much as possible about the behavior of the protein during crystal growth experiments and to help us understand the function of the neurotoxin once the structure is determined, we have initiated simple kinetic assays to evaluate the neurotoxins proteolytic activity. The substrate being used is a 17 amino acid peptide of the synaptic vesicle protein SNAP-25. After several months of attempting to optimize proteolytic activity, it was determined that the zinc concentration of the toxin must be 100 micromolar. If the concentration of any zinc salt is above the micromolar range, the neurotoxin activity is inhibited. If the concentration of any zinc salt is below the micromolar range, the neurotoxin activity is very low (less than 10% of full activity). With this information, we now routinely use 100 μM zinc acetate in all crystallization conditions to help stabilize the neurotoxin. It cannot be overemphasized that micromolar concentrations of zinc are absolutely necessary for full activity. In similar zinc protease structures, it is observed that correct concentrations of zinc atoms can possess either structural/catalytic or both roles in aiding the proteolytic activity. In the case of botulinum neurotoxin, we believe zinc to play both roles since we have observed that zinc salts stabilize the crystal growth under the optimal conditions (micromolar).

Analogous to other crystal structure determinations, it has frequently been observed that inhibitors for enzymes aid in the stabilization of protein molecules by locking the enzyme into a single stable conformation. By using the above kinetic assay, we have been able to screen potential inhibitors of the neurotoxin to stabilize a single conformation. The inhibitors being investigated including peptide-like analogs synthesized by Professor Paul Bartlett in the Dept. of Chemistry of UC-Berkeley. Based on the protease recognition site, we are investigating the inhibitors Z-Ala-Gly-Phe-, Z-Phe-P-Leu-Ala-, Z-Gly-Ala-P-, and Cbz-Gly-P-Leu-Gly-. The "-P-" moiety is a phosphate backbone in place of the amide backbone that strengthens the peptide bond and does not allow cleavage by the protease. The inhibitor does however have the recognition elements that the neurotoxin binds.

3. Isolated Domains of Botulinum Neurotoxin Serotype A

Recombinant DNA work on serotype A domains to produce protein for crystallography experiments. High expression levels of the translocation domain of BT serotype A have been achieved and purified. The *E. coli* expressed protein is folded and appears to be composed of both α -helices and beta-sheets based on CD (circular dichroism) experiments conducted in my laboratory. Since the present crystals of botulinum neurotoxin diffract to 3.0 \AA resolution, we will be able to determine the 3-dimensional structure of the neurotoxin and observe secondary structure elements (α helices, beta strands, and beta sheets). It will be difficult to observe detailed side chain interactions of the smaller side chains (the larger side chains should easily be observable). In order to obtain a more detailed picture of the protein structure, recombinant DNA work on isolated domains (binding, translocation, catalytic) have been initiated with the goal of crystallizing the domains and determining the 3-D structure by x-ray crystallography. The approach of

"divide & conquer" has been used in numerous examples to determine the structure of regions of protein molecules (i.e. SH2 & SH3 domains of tyrosine kinases).

All work on this aspect of the project has been conducted by personnel supported by the Department of Chemistry at UC-Berkeley. Proper authorization to conduct recombinant DNA work on fragments of botulinum neurotoxin were obtained from the Biosafety Officer, Office of Environment, Health and Safety (see Annual Report from previous year).

This work is in line with goals C5 and C7 of the contracted work, to crystallize the isolated domains of botulinum neurotoxin. Large quantities of purified protein is required and a recombinant approach is being taken. The alternative approach is by purifying the light and heavy chains from one another. This approach would require twice or greater the amount of holo-neurotoxin plus purification. Secondly, it is impossible to separate the binding domain from the translocation domain in this fashion.

Relationship to Goals of Research

All work to date focuses on the single goal of determining the 3-D structure. Although numerous side projects have emerged (kinetic assay, binding assays, recombinant DNA work), all of these projects are to aid in the crystal structure determination goal. Furthermore, the information obtained during these studies will be mandatory in understanding the function of the neurotoxin once the structure is known. All of the side projects listed above have been completed by personnel not supported by this contract. The individuals supported by the contract work only on the crystal structure determination.

CONCLUSION

We have accomplished the primary objective outlined in the research contract - the three-dimensional structure determination of botulinum neurotoxin serotype A. We have cloned and expressed the isolated domains, and crystallized the translocation domain. We have crystallized two other serotypes of botulinum neurotoxin (serotype B and E). This work has opened the door to a great deal of future work on understanding how the molecule functions. Furthermore, the results open the door for the design of inhibitors for the toxins activity. Already, we can speculate how the translocation domain interacts with the membrane based on long helices analogous to the helices in influenza virus hemagglutinin. We have collected data on inhibitors and receptors bound to the toxin.

Overall structure of botulinum neurotoxin type A

The crystal structure of BoNT/A was determined by multiple isomorphous replacement (MIR) using five heavy-atom derivatives. Phases were further improved with solvent flattening to yield readily interpretable electron density maps. The model, which includes 99% of the amino acids, was refined to 3.2 Å with an R value of 20.0% and an R_{free} value of 27.9%. The BoNT/A molecule is approximately 45 Å × 105 Å × 130 Å and shows a linear arrangement of the three functional domains with no contact between the catalytic and binding domains. In general, the three functional domains are also structurally distinct. The exception is an unusual loop, or belt, from what has historically been considered part of the translocation domain, that wraps around the perimeter of the catalytic domain.

Receptor binding domain

The binding domain, overall 32 Å × 37 Å × 76 Å, appears as two distinct sub-domains roughly equal in size. Both sub-domains are predominantly composed of b-strands and are connected by one prominent a-helix. The N-terminal sub-domain has two seven-stranded b-sheets sandwiched together in a jelly roll motif with dimensions 32 Å × 37 Å × 38 Å. The C-terminal sub-domain has similar dimensions and adopts a modified b-trefoil fold with a six-stranded b-barrel next to the N-terminal jelly roll motif and a b-hairpin triplet capping the base of the domain. The entire binding domain tilts away from the long helical axis of the translocation domain such that there is no contact between the C-terminal sub-domain and the translocation domain and all of the surface loops are accessible for binding. The binding domain shares structural homology with the recently solved structure of the tetanus toxin binding domain with an rms deviation of 1.5 Å for 363 Ca positions. The major differences appear in the loops of the C-terminal sub-domain, where the longer loop lengths in the tetanus toxin sub-domain account for the domain's slightly longer length in primary sequence.

The first step in the intoxication mechanism is a binding event between the binding domain and the pre-synaptic nerve ending. The interaction with BoNT/A is proposed to occur through both a polysialoganglioside (G_{D1b} or G_{T1b}) and a yet unidentified protein receptor. The putative ganglioside binding site for tetanus neurotoxin, as assessed by photoaffinity labelling, is in a loop of the C-terminal sub-domain, and when overlayed with the BoNT/A holotoxin structure, is fully accessible. This could represent a general ganglioside binding site for all the clostridial neurotoxins. It is striking that both sub-

domains have structural homology with proteins known to interact with sugars as assessed using Dali, a three-dimensional search algorithm, and its ranked output according to Z-score. (The Z-score is the strength of structural similarity in standard deviations over the expected where pairs with $Z < 2$ are structurally dissimilar.) The top twelve proteins after tetanus toxin ($Z=26.3$) structurally similar to the N-terminal sub-domain are proteins known to interact with sugars (i.e. serum amyloid P (1sac-A, $Z=12.8$), b-glucanase (2ayh, $Z=11.1$), sialidase (1kit, $Z=8.9$), lectin (1led, $Z=8.8$)). Perhaps the most notable of these twelve are cryia (1ciy, $Z=5.2$) and insecticidal δ -endotoxin (1dlc, $Z=4.8$) which act by binding glycoproteins and creating leakage channels. These toxins have binding domains structurally similar to the N-terminal sub-domain of BoNT/A but dramatically different pore-forming domains. A Dali search of the C-terminal sub-domain reveals more sugar binding proteins (basic fibroblast growth factor (1bfg, $Z=9.1$), agglutinin (1jly-A, $Z=9.9$)) and the toxin abrin (1abr-B, $Z=8.8$). Both abrin and the related ricin bind their targets through a b-trefoil binding domain. The appearance of different subsets of the same structural motifs in different toxins could suggest a mechanism of evolution in which stable functional domains are assembled as modular units giving rise to toxicity.

Pore-formation and translocation domain

Following cell surface binding and receptor-mediated endocytosis of the neurotoxin, an acid-induced conformational change in the neurotoxin's translocation domain is believed to allow the translocation domain to penetrate the endosome and form a pore. The membrane interaction and pore formation is thought to facilitate the passage of the catalytic domain across the membrane into the cytosol. The details of how the translocation domain changes conformation at acidic pH to form a pore and how it can allow for the passage of a 50 kDa catalytic domain across the endosomal membrane are the least understood aspects of the intoxication mechanism. To date, most investigations of the translocation event in BoNT have assumed a similarity to other pH dependent a-helical pore-forming proteins: diphtheria toxin, colicin A, d-endotoxin, pseudomonas exotoxin, and Bcl-x_L. These proteins share a common structural motif in their pore forming domain, however this motif is not observed in the BoNT/A structure.

The translocation domain of BoNT/A wraps around the catalytic domain before forming its main body, a cylindrical shape with dimensions of $28 \text{ \AA} \times 32 \text{ \AA} \times 105 \text{ \AA}$. The most salient feature of the translocation domain is a pair of a-helices 105 Å long corresponding to residues 685-827. While unusual, long pairs of a-helices have been observed recently in the structures of colicin Ia and the nucleotide exchange factor GrpE. The helices, anti-parallel and amphipathic, twist around each other like a coiled coil but do not adhere to a strict heptad repeat. At both ends of this pair of helices, a shorter a-helix packs in parallel to the long helical axis. In addition, the domain has two strand-like sections which pack against the pair of a-helices in a parallel fashion. In an effort to identify the pore-forming segment of BoNT/A, the primary sequence was searched for predicted amphipathic helicity, and the candidate segment (residues 659-681) was shown to increase permeability of lipid bilayers. The present structure, solved at neutral pH, shows that none of this putative transmembrane segment is helical and that, in fact, part of it appears to be in one of the two strand-like segments packing against the long a-helices. This could indicate an area which will undergo structural changes with pH. However, the residues most likely to titrate over this pH range are the two histidines in the translocation

domain, which are located away from this region of the structure. His 551 and His 560 are located in a loop between the translocation domain belt and the main body of the translocation domain. This junction may play a role in exposing a hydrophobic segment of the protein or releasing the catalytic domain from the translocation domain. Regardless of the pore-forming segment location, it is clear that the translocation domain of BoNT/A is structurally distinct from the other pore-forming toxins. In fact, the long pair of α -helices with their triple helix bundles at either end bear more resemblance to the coiled coil viral proteins: HIV-1 gp41/GCN4, influenza hemagglutinin, and the MoMuLV TM fragment. These proteins do not translocate through pores but do have an acid-induced ability to undergo structural changes and penetrate membranes.

Catalytic domain

Either within the acidic endosome or upon exposure to the cytosol following translocation, the disulfide bond connecting the catalytic and translocation domains (Cys 429 to Cys 453) is reduced, and the catalytic domain is released into the cytoplasm. The catalytic domain, $55 \text{ \AA} \times 55 \text{ \AA} \times 62 \text{ \AA}$, is a mixture of both α -helix and β -strand secondary structure, in agreement with secondary structure predictions. The active site of the catalytic domain is buried $20-24 \text{ \AA}$ deep in the protein, has a negative surface charge, and is accessible by a channel, $\sim 12 \text{ \AA} \times 15 \text{ \AA} \times 35 \text{ \AA}$. In the dichain holotoxin, this channel is partially shielded from solvent by both the belt and the main body of the translocation domain.

The final mechanistic step in toxicity is the cleavage of a presynaptic protein by the BoNT zinc protease catalytic domain. The catalytic zinc atom represents the highest peak in the electron density maps and is visible in MIR maps contoured at 7.5 s. Amino acids with side chains closest to the zinc include His 222, Glu 223, His 226, Glu 261, and Tyr 365. While the presence of His 222, Glu 223, and His 226 was anticipated, this structure identifies Glu 261 as the fourth ligand, and may help resolve uncertainty in tetanus toxin where either Glu 269 or Glu 270 had been implicated. (Glu 269 and Glu 270 of tetanus toxin align to Glu 260 and Glu 261 of BoNT/A). Further, while the role of a tyrosine was anticipated, the structure indicates that it is the conserved Tyr 365 and not the conserved Tyr 232 which is within proximity to the zinc. While exact bond lengths and water molecules can not be confirmed at this resolution, the observed orientation of these residues support a model in which the His 222, His 226, and Glu 261 directly coordinate the zinc, and Glu 223 coordinates a water molecule as the fourth ligand. The Tyr 365 is $\sim 5 \text{ \AA}$ from the zinc (OH--Zn) and is more likely to be involved in secondary bonding networks or interaction with substrate. Dali, shows that the proteins with the most structural similarity to the catalytic domain are thermolysin (1hyt, Z=4.6) and leishmanolysin (1lml, Z=2.4), two other zinc proteases with the same conserved HEXXH sequence. The structural similarities are limited, however, to the helix containing the HEXXH sequence and a 4-stranded β -sheet buttressing the helix. Beyond this overlap, the BoNT/A catalytic domain has different secondary structure elements and connectivities.

The catalytic domain of BoNT/A is highly specific for the C-terminus of SNAP-25 and appears to require a minimum of 16 substrate amino acids for cleavage. This large substrate size requirement is unusual for metalloproteases. The molecular recognition properties between the toxin and SNAP-25 and the dependence of recognition on a specific substrate secondary structure is presently being investigated. The channel

(~12 Å x 15 Å x 35 Å) leading to the active site appears capable of accommodating 16 or more residues with the Gln-Arg cleavage site of SNAP-25 able to insert into the zinc catalytic site. Additionally, the high pI of SNAP-25's C-terminal tail suggests that the negatively charged surface observed near the active site could be critical in the docking of substrate. Interestingly, the active site is most accessible in the absence of the translocation domain. This structure, in which the translocation domain shields the active site in the unreduced holotoxin, explains the fact that the catalytic activity in *in vitro* experiments is greatly enhanced by reduction of the disulfide. This observation of an occluded active site, along with the characterization of the amino acid environment, will almost certainly benefit ongoing inhibitor design.

Future work on this project includes the refinement of the botulinum neurotoxin model with bound inhibitor and receptor. This information is critical to understand how to combat the toxins effects.

BIBLIOGRAPHY

Publications

F. Chen, G. Kuziemko, P. Amersdorfer, C. Wong, J.D. Marks, R.C. Stevens "Antibody Mapping to Domains of Botulinum Neurotoxin serotype A in the Complexed and Uncomplexed Forms" *Infection & Immunity* **65**, 1626 (1997).

R. Burkhard, F. Chen, G. Kuziemko, R.C. Stevens "Electron Density Projection Maps of the 900 kD Botulinum Neurotoxin Complex by Electron Crystallography" *J. Structural Biology* **120**, 78 (1997).

D.B. Lacy and R.C. Stevens "Recombinant Expression and Purification of the Botulinum Neurotoxin A Translocation Domain", *Protein Expression and Purification* **11**, 195 (1997).

F. Chen, G. M. Kuziemko, R.C. Stevens "Biophysical Characterization of the Stability of the 150-Kilodalton Botulinum Toxin, the Non-toxic Component, and the 900-Kilodalton Botulinum Toxin Complex Species" *Infection & Immunity* **66**, 2420 (1998).

B. Lacy, W. Tepp, B. DasGupta, R.C. Stevens "Three-dimensional Crystal Structure of Botulinum Neurotoxin and Implications in Toxicity" *in press Nature Structural Biology* (1998).

Meeting Presentations

"Structure of Botulinum Neurotoxin"

Interagency Botulism Meeting, Washington, D.C. November, 1997

"Structural Features of Botulinum Neurotoxin Serotype A toxicity"

Gordon Conference, July 1998.

"Structural Studies of Botulinum Neurotoxin"

DOD Bioscience Review, Washington, D.C. June, 1998

Personnel Conducting Research on the Project at Univ. California-Berkeley

Professor Raymond C. Stevens

Dr. Cara Marks

Dr. Hanne Merritt

Heather Manning

Borden Lacy

Alona Cohen

Personnel Conducting Research on the project at U. Wisconsin-Madison (sub-contract)

Bibhuti DasGupta

Bill Tepp

Mary Evenson

Antibody Mapping to Domains of Botulinum Neurotoxin Serotype A in the Complexed and Uncomplexed Forms

FLORA CHEN,¹ GEOFFREY M. KUZIEMKO,² PETER AMERSDORFER,³ CINDY WONG,³
JAMES D. MARKS,^{3*} AND RAYMOND C. STEVENS^{1,2*}

Graduate Group in Biophysics¹ and Department of Chemistry,² University of California, Berkeley, California 94720,
and Departments of Anesthesia and Pharmaceutical Chemistry, University of California, San Francisco,
San Francisco, California 94110³

Received 8 November 1996/Returned for modification 13 January 1997/Accepted 7 February 1997

The domain organization of the botulinum neurotoxin serotype A was studied by using antibody mapping of 44 monoclonal single-chain variable fragments. The analysis was carried out on (i) the individual domains of botulinum neurotoxin holotoxin (binding, translocation, and catalytic), (ii) botulinum neurotoxin holotoxin, (iii) the botulinum neurotoxin holotoxin in complex with the nontoxic portion, and (iv) botulinum neurotoxin holotoxin and nontoxic portion of the complex recombined in vitro. All 44 antibodies mapped to individual domains of botulinum neurotoxin. Forty of the 44 single-chain variable fragments bound the botulinum neurotoxin holotoxin relative to the isolated domains, suggesting that 4 epitopes are covered when the individual domains are in the holotoxin form. Only 20 of the antibodies showed a positive reaction to the toxin while in complex with the nontoxic portion. All of the covered epitopes were mapped to the binding domain of botulinum neurotoxin, which suggested that the binding domain is in direct contact with the nontoxic portion in the complex. Based on the antibody mapping to the different domains of the botulinum neurotoxin holotoxin and the entire complex, a model of the botulinum neurotoxin complex is proposed.

The anaerobic bacterium *Clostridium botulinum* produces seven serotypes of neurotoxin, classified A through G (26). The neurotoxin, serotype A, can be purified as a 900-kDa complex consisting of a 150-kDa toxic component (botulinum neurotoxin [BT]), and a 750-kDa nontoxic component (hemagglutinin [HA]) (3). The BT inhibits cholinergic vesicle docking at the neuromuscular junction, resulting in flaccid paralysis (23), and most commonly intoxicates by oral ingestion. The three 50-kDa functional domains of BT—binding (13), translocation (2), and catalytic (1a)—allow the toxin to bind to a cell surface receptor, pass across the membrane (23), and cleave a protein involved in vesicle docking, respectively (9). Sugii and coworkers (24) have shown that the HA-BT complex has a higher oral toxicity in rats than the BT alone. The 750-kDa HA has been shown to have an agglutination ability (15) and is thought to protect the toxin from the extreme pH and proteases in the gut (25).

Little structural information is known about BT, HA-BT, or the interaction between BT and HA. The literature contains examples of antibodies used to detect various serotypes of BT (7, 12, 14, 27), but no mapping of the BT domains in the HA-BT complex has been carried out. Sugiyama and coworkers (27) showed that polyclonal antibodies to type A HA-BT complex recognized epitopes predominantly from the HA and not the BT. Monoclonal antibodies developed by Kozaki and coworkers recognized the light chain of the BT that causes infant botulism and the light chain of BT serotype A (14). However, the antibodies to the infant botulism BT heavy chain did not recognize the BT serotype A heavy chain. Studies using

polyclonal antibodies to the toxin detected BT at very low concentrations but did not provide specific information about the relationship between the BT and HA (7, 12). We probed the structure of the HA-BT complex by using a panel of 44 unique monoclonal single-chain variable fragments (scFv) derived from combinatorial phage antibody libraries (1, 28).

We used enzyme-linked immunosorbent assays (ELISAs) to identify 44 scFv that bind to different domains of botulinum neurotoxin serotype A. ELISAs were performed on purified BT, the purified BT domains, HA, HA-BT complex, and recombined HA-BT in vitro. Based on our results, we propose a model to illustrate the interaction between BT and HA. The model could act as a guide for the design of neutralizing antibodies and may explain how the HA protects the BT from proteolytic and pH attack.

MATERIALS AND METHODS

Purification of HA-BT complex, BT, and BT domains. The HA-BT complex (Hal strain) was obtained as an ammonium sulfate precipitate from purified bacterial supernatant at a concentration of 3.3 mg/ml in 50 mM sodium citrate (pH 5.5) (5). Before use, the HA-BT complex was centrifuged at 26,890 \times g (Dupont Sorvall RC-5B centrifuge) for 15 min and dialyzed against saline (0.68 M sodium citrate, 0.145 M NaCl [pH 7.4]) with three buffer exchanges within an hour. Concentration was determined by A_{278} measurements (1.66 arbitrary units/mg ml⁻¹) using a Shimadzu UV-160 spectrophotometer (11).

The HA was purified in two steps by using a modification of a published procedure (4). Forty-five milligrams of ammonium sulfate precipitate of HA (0.42 g/ml) was centrifuged at 26,890 \times g. The pellet was dissolved in 20 ml of 70 mM Tris-HCl (pH 7.2) and dialyzed overnight. The dialyzed solution was centrifuged at 26,890 \times g for 15 min and applied onto a DEAE-Sephadex column (1.5 by 24 cm; Pharmacia, Uppsala, Sweden) that was equilibrated with 70 mM Tris-HCl (pH 7.2). The column was washed with 100 ml of 70 mM Tris-HCl (pH 7.2) and the HA was eluted with 70 mM Tris-HCl–0.2 M NaCl (pH 7.2). The fractions containing HA were combined and run on an SP-Sephadex column (1.5 by 21 cm) (Pharmacia, Uppsala, Sweden) equilibrated with 70 mM Tris-HCl (pH 7.2). Since residual BT adheres to the column matrix at this pH, the HA was collected in the flowthrough. The concentration of protein was determined by A_{278} measurements (11).

The BT was purified as described previously (5) and stored as a 10-mg/ml solution in 10 mM HEPES (pH 7.0)–0.1 M KCl–2 mM sodium azide. The binding domain of BT type A, expressed in *Escherichia coli* and purified by immobilized metal affinity chromatography using a C-terminal His₆ tag, was

* Corresponding author. Mailing address for James D. Marks: Departments of Anesthesia and Pharmaceutical Chemistry, University of California, San Francisco, SFGH Room 3C-38, 1001 Potrero, San Francisco, CA 94110. Phone: (415) 206-3256. Fax: (415) 206-3253. E-mail: jim.marks@quickmail.ucsf.edu. Phone for R. C. Stevens: (510) 643-8285. Fax: (510) 643-9290. E-mail: Stevens@adrenaline.berkeley.edu.

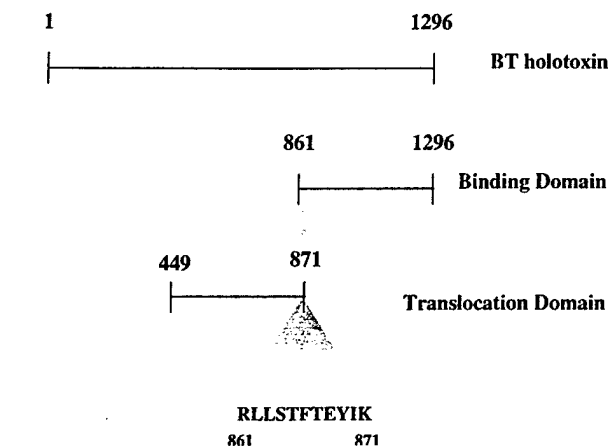


FIG. 1. Diagram illustrating the sequence overlap between the translocation and binding domain constructs. The top line represents the sequence of BT from the N terminus (residue 1) to the C terminus (residue 1296). The bottom two lines depict the C-terminal 11 residues from the translocation domain construct overlapping the N-terminal 11 residues of the binding domain (18, 19).

purchased from Ophidian Pharmaceuticals, Inc. (Madison, Wis.). The translocation domain (residues 449 to 872) of BT type A was expressed in *E. coli* and purified by immobilized metal affinity chromatography using a C-terminal His₆ tag (14a). The 11 C-terminal residues of the translocation domain overlap the 11 N-terminal residues of binding domain (18, 19) (Fig. 1). The polypeptide composition of each of the different batches of purified protein was analyzed on 12% polyacrylamide gels as described by Fling and Gregerson (8).

Antibodies. scFv antibody fragments were selected from four different combinatorial phage antibody libraries (1, 28). Briefly, scFv phage antibody libraries were constructed from the immunoglobulin heavy (V_H)- and light (V_L)-chain variable regions of mice immunized with purified holotoxin (library 1); mice immunized with binding domain (library 2); humans immunized with pentavalent botulinum toxoid (Centers for Disease Control and Prevention) (library 3); nonimmunized human volunteers (library 4). Libraries 1 and 3 were constructed in the vector pCANTAB5E (Pharmacia), and library 2 was constructed in pHEN-1 (10). Specific scFv were isolated by selecting the libraries on either holotoxin or binding domain immobilized on polystyrene or in solution. The specificity of the isolated antibodies for the holotoxin or the binding domain was confirmed by ELISA on the relevant antigen and a panel of irrelevant antigens (1, 28). The number of unique scFv was determined by *Bs*N1 fingerprinting, followed by DNA sequencing of the V_H and V_L genes. Additional unique scFv were isolated from a 9.7×10^9 -member nonimmune library in pHEN-1 (10) constructed from human V_H and V_L genes.

For structural mapping of the HA-BT complex, BT, and BT domains by ELISA, native scFv was expressed from the appropriate phagemid in *E. coli* HB2151 (10). The amber codon between the scFv gene and gene 3 permits expression of native scFv in a nonsuppressor *E. coli* strain (HB2151). scFv binding was detected by using the epitope tag at the C terminus of the scFv (E tag for scFv in pCANTAB5E and Myc tag for scFv in pHEN-1). Since both the scFv in pHEN-1 and the translocation domain have a C-terminal Myc tag, ELISA on the translocation domain was performed with scFv fused to phage, and detection was achieved by using HRP/anti-M13 conjugate (Pharmacia).

Expression of native scFv (6) in the phagemid vectors (pHEN-1 and pCANTAB5E) was performed in 96-well microtiter plates as described previously (16), with the following exception: after overnight growth and expression at 25°C, 50 µl of 0.5% Tween 20 was added to each well and the plates were incubated for 4 h at 37°C with shaking to induce bacterial lysis and increase the concentration of scFv in the bacterial supernatant. Supernatants containing native scFv were used for ELISA. To prepare phage for ELISA, single ampicillin-resistant colonies were transferred into microtiter plate wells containing 100 µl of 2× YT medium (16 g of Bacto Tryptone, 10 g of Bacto Yeast Extract, 5 g of NaCl, 1 liter of deionized H₂O) supplemented with 1 mM ampicillin (Sigma, St. Louis, Mo.) and 0.1% glucose. After 3 h of growth at 37°C to an A_{600} of approximately 0.5 arbitrary unit, VCSM13 helper phage (2.5 × 10⁸ phage particles) was added, and the cells were incubated for 1 h at 37°C. Subsequently, kanamycin was added to a final concentration of 25 µg/ml, and the bacteria were grown overnight at 37°C. Supernatants containing phage were used for ELISA.

ELISA. Microtiter plates (Falcon 3912) were incubated with 50 µl of antigen (10 µg/ml except for the binding domain, in which case 5 µg/ml was used) in phosphate-buffered saline (PBS; 25 mM NaH₂PO₄, 125 mM NaCl [pH 7.0]) at 4°C overnight. After being washed once with PBS, wells were incubated with 50 µl of bacterial supernatant containing either native scFv or scFv fused to phage. Myc-tagged scFv were detected with mouse monoclonal antibody 9E10 (1 µg/ml;

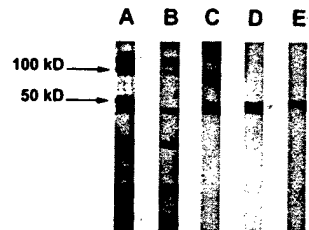


FIG. 2. SDS-PAGE analyses of column chromatography. Lanes: A, HA-BT complex; B, purified HA; C, purified BT; D, purified binding domain; E, purified translocation domain.

Santa Cruz Biotechnology) (17), and E-tagged scFv were detected by using anti-E tag antibody (1 mg/ml; Pharmacia), followed by peroxidase-conjugated anti-mouse Fc antibody (Sigma), with 2,2'-azinobis(3-ethylbenzothiazoline-sulfonic acid) as the substrate as described previously (21). Binding of scFv phage to antigens was detected with peroxidase-conjugated anti-M13 antibody (Pharmacia) as described elsewhere (20).

Recombination. The purified BT and HA were incubated at a 1:1 molar ratio for at least 24 h in 70 mM Tris-HCl (pH 7.2) at a protein concentration of 0.1 mg/ml. The mixture was stored at 4°C until diluted in PBS for coating ELISA plates.

RESULTS

Purification of antigens. After column chromatography, the purities of HA-BT complex, BT, and HA were ascertained by sodium dodecyl sulfate-polyacrylamide gel electrophoresis (SDS-PAGE) to be relatively free of contaminants (Fig. 2). The BT appeared as two bands, separated due to the reducing environment of the gel loading buffer—a 50-kDa light chain consisting of catalytic domain and a 100-kDa heavy chain consisting of translocation and binding domains. The HA-BT complex runs as nine bands that make up the BT and large HA. Purified HA appears identical to the HA-BT complex minus the 50-kDa polypeptide from the light chain of BT. A small amount of 100-kDa band from the heavy chain of BT was present in the HA. This residual BT was not enough to produce a positive signal for HA on ELISA. Binding and translocation domains, expressed in *E. coli* were also tested for purity by SDS-PAGE.

Antibody isolation and initial characterization. scFv were isolated by selection of phage libraries on immobilized purified BT or purified recombinant binding domain. The antibodies recognize only native protein and not denatured protein. Thus, the antibodies bound according to structure and not sequence libraries (1, 28). After three rounds of selection, initial scFv characterization by ELISA on BT and DNA sequencing of the V_H and V_L genes yielded 44 unique scFv (Table 1).

Structural mapping of BT, HA-BT complex, and BT domains. The forty-four scFv recognized the individual domains of BT, and none bound to HA alone (Table 1). Of the 44 scFv, 24 mapped to the binding domain and 3 mapped to the translocation domain (Table 1). In addition, two antibodies mapped to both the binding and translocation domains. These two scFv presumably bound to the 11-amino-acid overlap at the C terminus of the translocation domain and the N terminus of the binding domain (Fig. 1). Alternatively, cross-reactivity could result from binding to a four-amino-acid sequence (-KYVD-) that is homologous for residues 855 to 858 of the translocation domain and 1121 to 1124 of the binding domain. Thus, 26 scFv recognized the binding domain and 5 bound the translocation domain construct. The remaining 15 scFv presumably bound to the catalytic domain, though this was not tested directly due to lack of purified catalytic domain. Some of these 15 may recognize epitopes that are shared between domains.

TABLE 1. ELISA absorbances of scFv to type A neurotoxin^a

Antibody	OD ₄₀₅ (avg ± SD)				
	BT	HA-BT	Binding domain	Translocation domain	RR
3d12	2.303 ± 0.682	0.659 ± 0.072	2.260 ± 0.489		1.181 ± 0.303
3a6	2.053 ± 0.768	0.660 ± 0.083	1.775 ± 0.263		1.160 ± 0.322
3d4	0.964 ± 0.192	0.913 ± 0.192			1.091 ± 0.108
4a4	0.950 ± 0.135	0.905 ± 0.045			1.195 ± 0.071
3a2	1.091 ± 0.192	0.936 ± 0.138			1.204 ± 0.234
3e3	1.106 ± 0.170	0.987 ± 0.158			1.229 ± 0.255
3e8	1.058 ± 0.358	0.941 ± 0.097			1.145 ± 0.245
3a11	1.036 ± 0.298	0.934 ± 0.108			1.248 ± 0.157
3e7	1.022 ± 0.262	0.945 ± 0.156			1.218 ± 0.153
3h3	1.143 ± 0.396	0.838 ± 0.380			1.037 ± 0.316
3a1	1.019 ± 0.300	0.943 ± 0.148			1.206 ± 0.167
w3	2.083 ± 0.523	1.544 ± 0.192			1.925 ± 0.267
w42	1.796 ± 0.409	1.400 ± 0.223			1.721 ± 0.270
g23	1.875 ± 0.403	1.460 ± 0.194			1.795 ± 0.183
g3	1.287 ± 0.329	0.890 ± 0.298			1.290 ± 0.174
g11	1.200 ± 0.326	0.956 ± 0.192			1.285 ± 0.100
w7	1.552 ± 0.269	1.199 ± 0.273		1.182 ± 0.121	1.606 ± 0.393
w9	1.492 ± 0.376	1.239 ± 0.247		1.201 ± 0.152	1.510 ± 0.194
g7	1.072 ± 0.481	1.106 ± 0.327		0.590 ± 0.105	1.422 ± 0.261
w20	1.557 ± 0.530		1.713 ± 0.349		1.089 ± 0.053
w36	1.302 ± 0.418		1.362 ± 0.300		0.680 ± 0.026
w43	1.421 ± 0.253	1.002 ± 0.109			1.283 ± 0.334
g53	1.193 ± 0.321		1.700 ± 0.242		0.685 ± 0.095
g57	1.647 ± 0.409		1.423 ± 0.521		0.761 ± 0.117
c9	1.560 ± 0.460		1.690 ± 0.229		0.889 ± 0.213
c15	1.936 ± 0.535		1.988 ± 0.458		1.079 ± 0.358
s25	1.395 ± 0.363		1.369 ± 0.435		0.811 ± 0.142
3f6	1.332 ± 0.338		1.553 ± 0.272		0.838 ± 0.033
2a2	0.816 ± 0.297		1.172 ± 0.262		0.661 ± 0.143
2b10	0.858 ± 0.332		1.204 ± 0.408		0.566 ± 0.010
2b1	0.836 ± 0.121		1.247 ± 0.278	1.227 ± 0.505	0.605 ± 0.165
3e6	0.909 ± 0.109		1.190 ± 0.135		
2e6	0.838 ± 0.181		1.046 ± 0.171		
3d1	0.908 ± 0.192		1.009 ± 0.385		0.752 ± 0.072
2b6	0.652 ± 0.298		0.711 ± 0.213		
2h6	1.010 ± 0.326		1.261 ± 0.346		0.928 ± 0.004
2a8	0.994 ± 0.275		1.069 ± 0.398		0.908 ± 0.226
id5	0.738 ± 0.289		1.273 ± 0.228		0.716 ± 0.085
ic8	0.556 ± 0.339		0.921 ± 0.513	1.000 ± 0.405	0.654 ± 0.057
ig7	0.834 ± 0.174		1.113 ± 0.313		0.688 ± 0.077
3c3			0.621 ± 0.026		
2c3			0.740 ± 0.065		
3c2			0.427 ± 0.089		
3c5			0.743 ± 0.204		

^a Values obtained with antigen coated at 10 µg/ml except for the binding domain, which was coated at 5 µg/ml. OD₄₀₅, optical density at 405 nm; RR, recombination of purified BT and HA. The antibodies were produced in the lab of James D. Marks. The values represent the averages of 13 plates coated with BT, 10 plates coated with HA-BT complex, 6 plates coated with binding domain, 6 plates coated with translocation domain, 5 plates coated with HA, and 4 plates coated with recombinant BT and HA. The background was defined as the signal from plates containing antigen and primary and secondary antibodies. Values represent absorbances after background absorbance is subtracted. Blanks in columns represent absorbances below three times the background absorbance. These scFv were assumed not to bind the corresponding antigen. Since the ELISAs were performed using different batches of supernatant, the average absorbance of each plate was normalized to the average absorbance of the first plate for a particular antigen.

Forty scFv bound to the holotoxin (Table 1). Thus, four epitopes were covered when the individual domains came together to form the BT. Of these 40 scFv, 22 mapped to the binding domain and 3 mapped to the translocation domain. The remaining 15 scFv were deduced to recognize the catalytic domain (Table 1).

ELISA of scFv on the HA-BT complex permitted identification of BT epitopes which were inaccessible in the HA-BT complex. Twenty epitopes were covered when in the HA-BT complex. All of these covered epitopes were localized to the binding domain. Of the 22 scFv that mapped to the binding domain and BT, only 2 scFv bound to the HA-BT complex

(Table 1). The three scFv that bound to translocation domain and BT also bound to the HA-BT complex (Table 1). The 15 scFv that mapped to catalytic domain in BT likewise bound to the HA-BT complex (Table 1).

DISCUSSION

Using antibodies to map the different domains of botulinum neurotoxin serotype A, we propose a model illustrating how the toxin may bind into the HA assembly. Forty-four scFv were produced to the BT and its domains. The antibodies specific to individual domains were used to map relative positions of

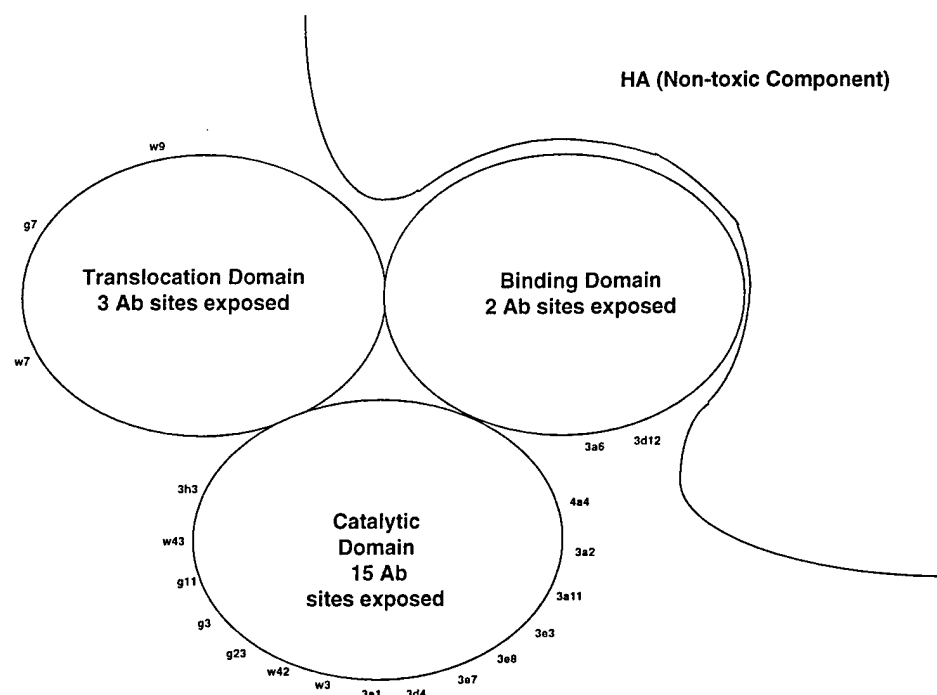


FIG. 3. Representation of a possible arrangement of BT with respect to HA. Only clones which bind the HA-BT complex are shown. The binding and translocation domains are covered partially by HA. Ab, antibody.

exposed or hidden epitopes in the BT and in the HA-BT complex. All of the antibodies specific to the translocation domain also recognized the HA-BT, indicating that the translocation domain is as exposed to the solvent in the complex (Fig. 3) as in the holotoxin (Table 1).

Not all of the scFv which bound the individual domains bound the BT holotoxin. Twenty-two of the 26 antibodies that recognized binding domain also recognized the BT. Thus, 4 antibody sites on the binding domain are covered by the catalytic or translocation domain in the BT (Table 1). However, not all of these scFv bound when the BT was complexed with the HA. Of the 22 exposed sites of binding domain on BT, only 2 bound the HA-BT complex. Therefore, the majority of antibodies to the binding domain recognize epitopes that must be covered by HA in the HA-BT complex (Fig. 3).

Fifteen antibodies were deduced to bind the catalytic domain. These antibodies were inferred by subtracting the antibodies that bound the binding and translocation domains from the antibodies that bound BT, since it is assumed that all of the antibodies must bind a domain of BT. All of these 15 antibodies bind an epitope that is accessible in the HA-BT complex. These 15 antibodies may bind conformational epitopes shared between domains. Such epitopes may not exist in the separate domains.

The model illustrated in Fig. 3 is subject to several caveats. Since the sequences of the epitopes are unknown, it is not possible to know the distribution of antibody binding sites. Hence the epitopes could be distributed evenly on the exposed surfaces or could be concentrated in certain regions of the protein. If the epitopes are clustered together, the area of BT covered by HA may be overestimated. If the epitopes are spaced regularly, the area of BT covered by HA may be underestimated. In either case, verification requires mapping of these antibodies to specific sequences of BT. Finally, since the model is drawn in two dimensions, it may not depict accurately

the surface area of BT covered by HA. In addition, the arrangement of exposed and unexposed epitopes may be different from that diagrammed. The representation shows contiguous groups of exposed or unexposed epitopes that may be commingled.

The recombination experiments were performed to determine whether purified BT would interact with purified HA to reform the stable HA-BT complex at physiological pH. Since HA was undetectable by any of the antibody clones, the clones that bound to recombined HA-BT must bind exposed regions of BT. If no reconstitution of the complex occurred, recombinant HA-BT should show the same number of clones as purified BT. If the HA-BT complex was formed, then recombinant HA-BT should exhibit a positive reaction with the same clones as the purified HA-BT complex. The results from Table 1 indicate that an incomplete recombination took place. Whereas 40 clones recognized BT and 20 clones recognized the HA-BT complex, 37 clones bound recombinant HA-BT. The three clones found in recombinant HA-BT but not in the BT complex (s25, 2e6, and 2b6) are specific to the binding domain. Thus, under the recombination conditions, BT and HA do not fully reassemble. Some of the binding domain is left uncovered by HA.

Surprisingly, all of the epitopes that were covered in the HA-BT complex were mapped to the binding domain, strongly suggesting that the interactions between HA and BT are mediated by the binding domain. This idea is biologically relevant, since uncomplexed BT is susceptible to trypsin cleavage at the binding domain (22). Furthermore, the trypsinized BT could not bind to brain synaptosomes. When uncomplexed BT was incubated with trypsin, the translocation and catalytic domains showed no sign of proteolysis. Therefore, in the HA-BT complex, the HA may protect the binding domain of BT from proteolytic attack. These observations may guide in developing

antibodies for therapeutic design of neutralizing antibodies against botulism poisoning.

ACKNOWLEDGMENTS

We thank Bill Tepp and Bibhuti DasGupta, Department of Food Microbiology and Toxicology, University of Wisconsin, Madison, for generous supplies of BT and HA-BT complex. Also, we thank Birgitte Andersen for a careful reading of the manuscript.

We gratefully appreciate the support of U.S. Department of Army contracts DAMD17-93-C-3118 and DAMD17-94-C-4034.

REFERENCES

- Amersdorfer, P., et al. Unpublished data.
- Blaesi, J., E. R. Chapman, E. Link, T. Binz, S. Yamasaki, P. De Camill, T. C. Südhof, H. Niemann, and R. Jahn. 1993. Botulinum neurotoxin A selectively cleaves the synaptic protein SNAP-25. *Nature* **365**:160–163.
- Blauestein, R. O., W. J. Germann, A. Finklestein, and B. R. DasGupta. 1987. The N-terminal half of the heavy chain of botulinum type A neurotoxin forms channels in planar phospholipid bilayers. *FEBS Lett.* **226**:115–120.
- DasGupta, B. R., and D. A. Boroff. 1968. Separation of toxin and hemagglutinin from crystalline toxin of *Clostridium botulinum* type A by anion exchange chromatography and determination of their dimensions by gel filtration. *J. Biol. Chem.* **243**:1065–1072.
- DasGupta, B. R., D. A. Boroff, and E. Rothstein. 1966. Chromatographic fractionation of the crystalline toxin of *Clostridium botulinum* type A. *Biochem. Biophys. Res. Commun.* **22**:750–756.
- DasGupta, B. R., and V. Sathyamoorthy. 1984. Purification and amino acid composition of type A botulinum neurotoxin. *Toxicon* **22**:415–424.
- De Bellis, D., and I. Schwartz. 1990. Regulated expression of foreign genes fused to lac: control by glucose levels in growth medium. *Nucleic Acids Res.* **18**:1311.
- Ekong, T. A. N., K. McLellan, and D. Sesardic. 1995. Immunological detection of *Clostridium botulinum* toxin type A in therapeutic preparations. *J. Immunol. Methods* **180**:181–191.
- Fling, S. P., and D. S. Gregerson. 1986. Peptide and protein molecular weight determination by electrophoresis using a high-molarity Tris buffer system without urea. *Anal. Biochem.* **155**:83–88.
- Hayashi, T., H. McMahon, S. Yamasaki, T. Binz, Y. Hata, T. C. Südhof, and H. Niemann. 1994. Synaptic vesicle membrane fusion complex: action of clostridial neurotoxins on assembly. *EMBO J.* **13**:5051–5061.
- Hoogenboom, H. R. 1991. Multisubunit proteins on the surface of filamentous phage: methodologies for displaying antibody (Fab) heavy and light chains. *Nucleic Acids Res.* **19**:4133–4137.
- Knox, J. N., W. P. Brown, and L. Spero. 1970. The role of sulfhydryl groups in the activity of type A botulinum toxin. *Biochim. Biophys. Acta* **214**:350–354.
- Kozaki, S., Y. Kamata, T. Nagai, J. Ogasawara, and G. Sakaguchi. 1986. The use of monoclonal antibodies to analyze the structure of *Clostridium botulinum* type E derivative toxin. *Infect. Immun.* **52**:786–791.
- Kozaki, S., A. Miki, Y. Kamata, T. Nagai, J. Ogasawara, and G. Sakaguchi. 1989. Immunological characterization of papain-induced fragments of *Clostridium botulinum* type A neurotoxin and interaction of the fragments with brain synaptosomes. *Infect. Immun.* **57**:2634–2639.
- Lacy, B. Unpublished data.
- Lamanna, C. 1948. Hemagglutination by botulinal toxin. *Proc. Soc. Exp. Biol. Med.* **69**:332–336.
- Marks, J. D., H. R. Hoogenboom, T. P. Bonnert, J. McCafferty, A. D. Griffiths, and G. Winter. 1991. By-passing immunization. Human antibodies from V-gene libraries displayed on phage. *J. Mol. Biol.* **222**:581–597.
- Munro, S., and H. R. Pelham. 1986. An HSP70-like protein in the ER: identity with the 78 kDa glucose-regulated protein and immunoglobulin heavy chain binding protein. *Cell* **46**:291–300.
- Sathyamoorthy, V., B. R. DasGupta, J. Foley, and R. L. Niece. 1988. Botulinum neurotoxin type A: cleavage of the heavy and light chains into two halves and their partial sequences. *Arch. Biochem. Biophys.* **266**:142–151.
- Sathyamoorthy, V., B. R. DasGupta, and R. L. Niece. 1986. Botulinum neurotoxin type A: cleavage and partial sequence of the H chain. *Fed. Proc.* **45**:1793.
- Schier, R., R. F. Balint, A. McCall, G. Apell, J. W. Lerrick, and J. D. Marks. 1996. Identification of functional and structural amino-acid residues by parsimonious mutagenesis. *Gene* **169**:147–155.
- Schier, R., J. Bye, G. Apell, A. McCall, G. P. Adams, M. Malmquist, L. M. Weiner, and J. D. Marks. 1996. Isolation of high-affinity monomeric human anti-c-erbB-2 single chain Fv using affinity-driven selection. *J. Mol. Biol.* **255**:28–43.
- Sheets, M. Unpublished data.
- Shone, C. C., P. Hambleton, and J. Melling. 1985. Inactivation of *Clostridium botulinum* type A neurotoxin by trypsin and purification of two tryptic fragments. *Eur. J. Biochem.* **151**:75–82.
- Simpson, L. L. 1980. Kinetic studies on the interaction between botulinum toxin type A and the cholinergic neuromuscular junction. *J. Pharmacol. Exp. Ther.* **212**:16–21.
- Sugii, S., I. Ohishi, and G. Sakaguchi. 1977. Correlation between oral toxicity and in vitro stability of *Clostridium botulinum* type A and B toxins of different molecular sizes. *Infect. Immun.* **16**:910–914.
- Sugii, S., I. Ohishi, and G. Sakaguchi. 1977. Intestinal absorption of botulinum toxins of different molecular sizes in rats. *Infect. Immun.* **17**:491–496.
- Sugiyama, H. 1980. *Clostridium botulinum* neurotoxin. *Microbiol. Rev.* **44**:419–448.
- Sugiyama, H., I. Ohishi, and B. R. DasGupta. 1974. Evaluation of type A botulinum toxin assays that use antitoxin to crystalline toxin. *Appl. Microbiol.* **27**:333–336.
- Wong, C., et al. Unpublished data.

Editor: A. O'Brien

Electron Density Projection Map of the Botulinum Neurotoxin 900-kilodalton Complex by Electron Crystallography

Frederick Burkard

Lawrence Berkeley National Laboratory, Berkeley, California 94720

Flora Chen

Graduate Group in Biophysics, University of California, Berkeley, California 94720

Geoffrey M. Kuziemko

Department of Chemistry, University of California, Berkeley, California 94720

and

Raymond C. Stevens¹

Lawrence Berkeley National Laboratory, Berkeley, California 94720; and Graduate Group in Biophysics and Department of Chemistry, University of California, Berkeley, California 94720

Received July 24, 1997, and in revised form July 31, 1997

INTRODUCTION

The 900-kDa botulinum neurotoxin complex serotype A has been crystallized by the lipid-layer two-dimensional crystallization technique. Based on the binding characteristics of the hemagglutinating portion of the complex, a number of ganglioside/lipid mixtures were tested but only lactosyl ceramide/1-palmitoyl-2-oleoyl-sn-glycero-3-phosphocholine was found to crystallize the complex. The optimum lipid mixture contained 75 mass % lactosyl ceramide and 25 mass % 1-palmitoyl-2-oleoyl-sn-glycero-3-phosphocholine. Using protein concentrations from 5 to 500 µg/ml and pH 5 acetate buffer, we have obtained crystals that diffract to better than 15 Å when prepared in negative stain. A projection map with a resolution of 30 Å was calculated with unit cell dimensions of $a = b = 157 \text{ Å}$ and $P3$ symmetry. The complex is triangular in shape with six distinct lobes observed. Additionally, six smaller structures protrude from the triangular core. © 1997 Academic Press

Botulinum neurotoxin complex serotype A is a 900-kDa protein produced as one of eight serotypes (A-G) by the anaerobic bacterium *Clostridium botulinum*. Among the most potent biological toxins known, botulinum neurotoxin causes inhibition of synaptic vesicle release at the neuromuscular junction, resulting in flaccid paralysis (Simpson, 1980) and ultimately death. The 900-kDa complex contains a 150-kDa toxic component (BoNTA) and an ~750-kDa component (HA) (DasGupta and Boroff, 1968). Under denaturing and reducing conditions, the complex runs as nine bands on polyacrylamide gels (DasGupta, 1980). The purified 150-kDa neurotoxin runs as a 100-kDa heavy chain and a 50-kDa light chain, which are linked by a disulfide bond under nonreducing conditions. The heavy chain contains the binding and translocation domains (Sugiyama, 1980) which bind to a cell surface receptor and allow the toxin to pass across the membrane, while the light chain contains the catalytic domain which cleaves a protein involved in synaptic vesicle docking (Hayashi *et al.*, 1994). The remaining seven bands of the complex make up the HA component which is nontoxic and has the ability to agglutinate cells. The

¹ To whom correspondence should be addressed at Department of Chemistry, University of California, Berkeley, Berkeley, CA 94720. Fax: (510) 643-9290. E-mail: stevens@adrenaline.berkeley.edu.

stoichiometry of subunits making up the HA is unclear. The nontoxic components (HA) of the complex are thought to aid the toxin during its travel through the harsh conditions of the gastrointestinal tract.

The HA binds tightly to certain sugars such as *o*-nitrophenyl-*b*-D-galactoside, isopropyl-*b*-D-thiogalactoside, and lactose (DasGupta and Sugiyama, 1977), consequently inhibiting its ability to agglutinate. Furthermore, the complex may be adsorbed onto a sugar affinity column and BoNTA eluted away from the HA by raising the pH from 6.3 to 7.9 (Moberg and Sugiyama, 1978). Several of the sugars recognized by HA appear as head groups on naturally occurring gangliosides, making them ideal candidates as the monolayer used in the two-dimensional lipid-layer crystallization. This method (Uzgiris and Kornberg, 1983) has been used for the crystallization of a number of soluble proteins at the air-water interface and has the advantage of allowing trials with a very small amount of protein over a wide range of buffer conditions. In general, the interaction with the protein is based on either a specific lipid head group such as biotinylated PE with streptavidin (Darst *et al.*, 1991) and GM-1 with cholera toxin (Mosser and Brisson, 1991) or more nonspecific electrostatic interactions such as octadecylamine with RNA polymerase (Darst *et al.*, 1988).

There have been several examples of two-dimensional crystallization of clostridial toxins. Boroff and co-workers (1972) have visualized two-dimensional crystals of the botulinum neurotoxin serotype A toxic and nontoxic components separately using electron microscopy. Botulinum neurotoxin serotype B has been crystallized on lipid layers containing the ganglioside GT1b (Morgan *et al.*, 1989). Schmid *et al.* (1993) visualized the toxic component of serotype B as ordered arrays of channels in phospholipid vesicles and performed a three-dimensional reconstruction. Robinson and co-workers (1988) crystallized tetanus toxin on phospholipid monolayers and performed a three-dimensional reconstruction to 14 Å. Although the botulinum neurotoxin complex readily forms three-dimensional needle-like crystals (Sugiyama *et al.*, 1977), larger crystals are needed for structure determination by X-ray crystallography. To our knowledge, no prior structural information has been published for the 900-kDa complex of botulinum neurotoxin.

After an initial screening of several gangliosides and commonly used lipids, we found that only lactosyl ceramide, a ganglioside with a lactose head group, induced the botulinum neurotoxin complex to crystallize. Subsequent experiments involved optimization of lipid mixtures, protein concentration, and subphase conditions. Two-dimensional crystals grown under optimized conditions were collected, and se-

lected images were processed and used to generate the projection maps presented in this work. Although spots visible to the eye extending to a resolution of 22 Å may be seen in the computed Fourier transform (Fig. 2A) the image processing software is able to identify spots with suitable signal-to-noise ratio to 14 Å resolution (Fig. 2B). Due to the relative scarcity of higher resolution spots and their low amplitudes, we believe that the projection maps that are presented more realistically represent the BoNTA-HA complex to a resolution of 30 Å.

MATERIALS AND METHODS

Botulinum toxin complex was obtained as an ammonium sulfate precipitate and purified as previously described (Chen *et al.*, 1997). The purity of the protein used for crystallization was verified by SDS-PAGE. Botulinum neurotoxin complex was dialyzed into 50 mM sodium acetate buffer, pH 5, 100 mM sodium chloride and stored at 1.5 mg/ml at 20°C (storage at 4°C causes irreversible sticking to the wall of the container; surprisingly, the complex is stable at 20°C for extended periods of time). Additionally, 10 mM citric acid, pH 5, 100 mM sodium chloride buffer was also used. All reagents were obtained from Fisher Scientific (Fair Lawn, NJ) unless otherwise noted. Crystallization of the complex was also attempted with 50 or 100 mM calcium chloride added to each buffer. Trials with buffer pHs of 4 to 9 were carried out in buffers containing 100 mM sodium chloride, 2 mM sodium azide. The following buffering agents were used: 10 mM citric acid (pH 4), 10 mM Bis Tris (pH 6), 10 mM Hepes (pH 7 and pH 8), and 10 mM CHES (pH 9). 1-Palmitoyl-2-oleoyl-sn-glycero-3-phosphocholine (POPC) was purchased from Avanti Polar Lipids, Inc. (Alabaster, AL) and stored as a 25 mg/ml stock solution in chloroform at -20°C. Lactosyl ceramide (LC) was purchased from Matreya, Inc. (Pleasant Gap, PA) and stored at 0.5 mg/ml in chloroform at -20°C. The lipid-ganglioside mixtures were 0.5 mg/ml in chloroform with lipid:ganglioside ratios of 100% POPC:0% LC, 95% POPC:5% LC, 90% POPC:10% LC, 80% POPC:20% LC, 70% POPC:30% LC, 60% POPC:40% LC, 50% POPC:50% LC, 35% POPC:65% LC, 25% POPC:75% LC, 15% POPC:85% LC, 0% POPC:100% LC. Crystallization with other gangliosides (Trisialganglioside GT1b, Monosialoganglioside GM1, globotriosyl ceramide, globotetraosyl ceramide GL-4) (Matreya, Inc.) was also attempted. Grids (300 mesh) (Electron Microscopy Sciences, Fort Washington, PA) were coated with carbon and rendered hydrophobic by glow discharge treatment at 0.20 Torr in an atmosphere of hexafluoropropylene (PCR Inc., Gainesville, FL).

Protein was diluted into the appropriate buffer to a concentration between 5 and 500 µg/ml and 20 µl was pipetted into Teflon wells 1 mm deep and 4 mm in diameter. Then 0.5 to 1 µl of lipid-ganglioside solution was placed on top of the protein drop (Darst *et al.*, 1988). Specimens were incubated for 36 to 48 hr at room temperature in a sealed chamber at high humidity to prevent evaporation. Shortly before harvesting, carbon-coated electron microscopy grids were rendered hydrophobic by glow discharge treatment as described above and placed horizontally onto the surface of the protein drop. The grid was removed from the surface of the drop, washed with 50 µl water, and stained with 50 µl 2% (w/v) uranyl acetate (Fluka, Ronkonkoma, NY) for approximately 90 sec.

All experiments were done at room temperature. Preliminary electron microscopy was performed on a Zeiss 10A at 80 kV. Micrographs used for image processing were recorded under low-dose conditions (approximately 10 electrons per Å²) at 40 000× magnification and 2 µm under focus on a Jeol 100B with a field emission gun at 100 kV on Kodak S0-163 film. The magnification

on the Jeol 100B was calibrated with a 2160 lines/mm replica grating and estimated to be $43\,900\times$ for the images recorded. Promising micrographs were selected by optical diffractometry. Eight regions on seven micrographs were scanned on a Perkin-Elmer PDS 1010M flat bed microdensitometer controlled by an IBM PC running software developed at LBNL. Images were recorded in arrays of 1000 by 1000 using a 20- μm square aperture. Calculation of the lattice parameters and projection map was done using standard methods (Crowther *et al.*, 1996). Structure factors from individual images were used in the final map only if their signal-to-background ratio was better than 2.5 to 1.

RESULTS

Once it was established that BoNTA-HA would crystallize under a monolayer of LC/POPC, a number of experiments were performed to determine the conditions for optimal size and coherence. In general the crystallization of BoNTA-HA was not especially sensitive to buffer pH, ionic strength, or protein concentration. Protein could be observed adsorbed to the lipid monolayer after 18 to 24 hr of incubation at room temperature and ordered arrays were found most reliably after 36 hr. The lipid composition, however, affected the quality and compactness of the crystalline patches. Lipid mixtures containing from 50 to 100% LC, protein concentrations of 5 to 500 $\mu\text{g}/\text{ml}$, and buffer pHs from 4 to 7 (100 mM salt) all yielded crystals that diffracted well. The best conditions were found to be a lipid composition of 75:25 LC to POPC, 7.5 $\mu\text{g}/\text{ml}$ BoNTA-HA, and pH 5 in acetate buffer.

Crystals obtained above pH 7 were smaller, were less compact, and diffracted poorly. It is known that the complex dissociates into BoNTA and HA above pH 7.9 (DasGupta and Boroff, 1968). Under the conditions of crystallization, the complex between BoNTA and HA should remain intact. The poor crystal quality seen above pH 7 may be attributed to the high polydispersity observed for the complex at high pH using dynamic light scattering (Chen *et al.*, 1997b).

Figure 1A is representative of the crystalline areas imaged by electron microscopy. As can be seen, the monomeric units are predominantly triangular. Although locally well ordered, there are still disordered regions in the surface, possibly due to imperfect transfer from the air-water interface to the carbon film of the grid. Also noticeable are portions of several lattice rows stained in such a way that they stand out from the rest of the array in Fig. 1A. Closer examination suggests that they are composed of structures different from the "triangles" making up the bulk of the array. Additionally, lattice rows crossing these boundaries typically appear to be shifted approximately $1/4$ to $1/3$ unit cell.

Figure 1B shows both partially formed crystals and what appear to be numerous monomers bound to the monolayer but not yet incorporated into the

lattice. As shown by the object circled in this figure, they appear to be composed of a central triangular shape similar in size and shape to the repeating unit seen in the crystal, but surrounded by six structures radiating from the center. Several individual units may be seen in Fig. 1C. Based on measurements on the micrograph, we estimate that these figures have an overall diameter of 200 to 250 \AA each. Since the crystalline repeat distance is of the order of 150 \AA , it is unclear as to what happens to the radiating structures when the monomer is incorporated into the lattice.

The area marked in Fig. 1D shows a region in which the protein seems to be interacting with the monolayer at two distinct orientations as evidenced by the alternating rows of triangular monomers and ladder-like shapes. This phenomenon gives rise to the striated appearance.

Figure 2A shows a typical computed diffraction pattern resulting from two cycles of correction for lattice distortions (Crowther *et al.*, 1996). The average lattice parameters are $a^* = 1/135 \pm 1/3 \text{\AA}^{-1}$, $b^* = 1/139 \pm 1/5 \text{\AA}^{-1}$, and $\gamma^* = 60^\circ \pm 2^\circ$. While there is always some difference in the length of the lattice vectors, we have not identified any features in the diffraction pattern or projection map consistent with the unique assignment of either vector. Based on the unit cell parameters and diffraction data, $P3$ symmetry is assumed at the present resolution. The highest resolution spots easily seen by eye in this pattern are at a resolution of approximately $1/22 \text{\AA}^{-1}$ (the -4,7, the 7,-3 and the 3,4 are circled). Figure 2B is a plot of the same data generated by the image processing software. The relative sizes of the circles represent the signal-to-noise ratio of the corresponding diffraction spots. Only spots with a signal-to-noise ratio of 2.5:1 or better are shown. The resolution of the outermost spots is at approximately $1/14 \text{\AA}^{-1}$. The circled spots are the same as in Fig. 2A. Data from seven additional images were processed for lattice distortions, corrected for contrast transfer function phase reversals, combined by vector addition, and weighted on the basis of phase agreement to generate the projection map shown in Fig. 3A. The average phase residual from the data used to generate this map is $18.8^\circ \pm 5.0^\circ$. The figure shows two by two unit cells with each parallelogram having cell parameters of $a = 155(\pm 3) \text{\AA}$, $b = 159(\pm 5) \text{\AA}$, and $\gamma = 120^\circ$. Figure 3B shows the same data with $P3$ symmetry imposed; the unit cell parameters are $a = b = 157 \text{\AA}$ and $\gamma = 120^\circ$ with a phase residual of $17.5^\circ \pm 4.1^\circ$.

Although the results indicate that relatively high-resolution information is present in the data, the amplitudes of the structure factors drop off rapidly at resolutions greater than $1/130 \text{\AA}^{-1}$. This is consistent with the detail seen in the projection maps. The

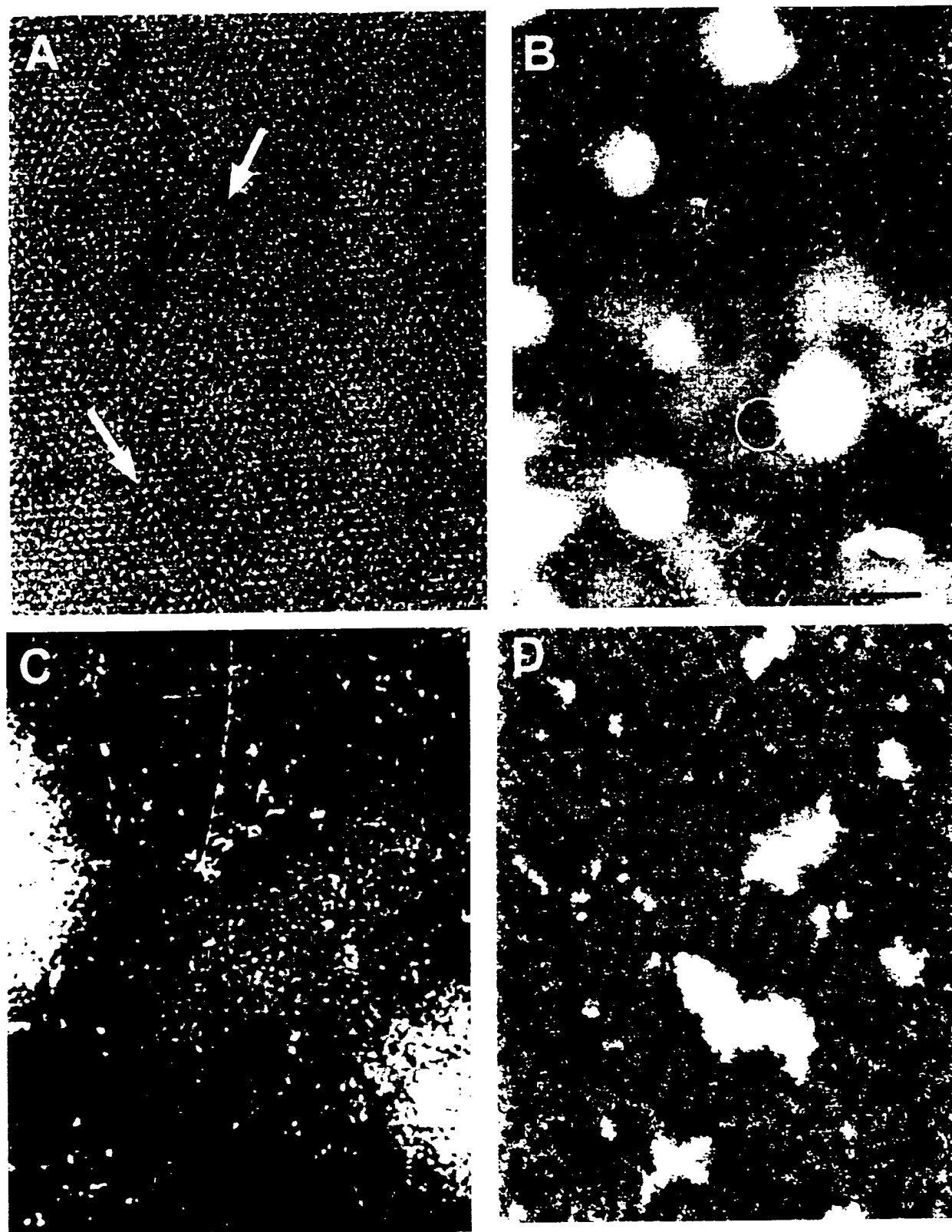


FIG. 1. Electron micrograph of lipid layers transferred to the EM grid and stained with uranyl acetate. BoNTA-HA complex in 100 mM sodium chloride, 50 mM sodium acetate buffer (pH 5.0) incubated with 3:1 (v/v) lactosyl ceramide: POPC. Bar represents 100 nm. (A) Two-dimensional crystal of botulinum neurotoxin complex. Arrows show lattice dislocations. (B) Monomers of protein adsorbed to monolayer both individually and incorporated into crystal. (C) Enlarged view of monomer unit. Note structures radiating from edges and sides of individual triangular units. (D) Alternating rows of triangular and ladder-like monomers.

sharpness of the visible spots seen in Fig. 2A and the number of reflections with good signal-to-noise ratios apparent in Fig. 2B led us to believe that crystals of the BoNTA-HA complex are locally quite well ordered. Improvements in the size of the crystal, elimination or avoidance of crystal defects, and

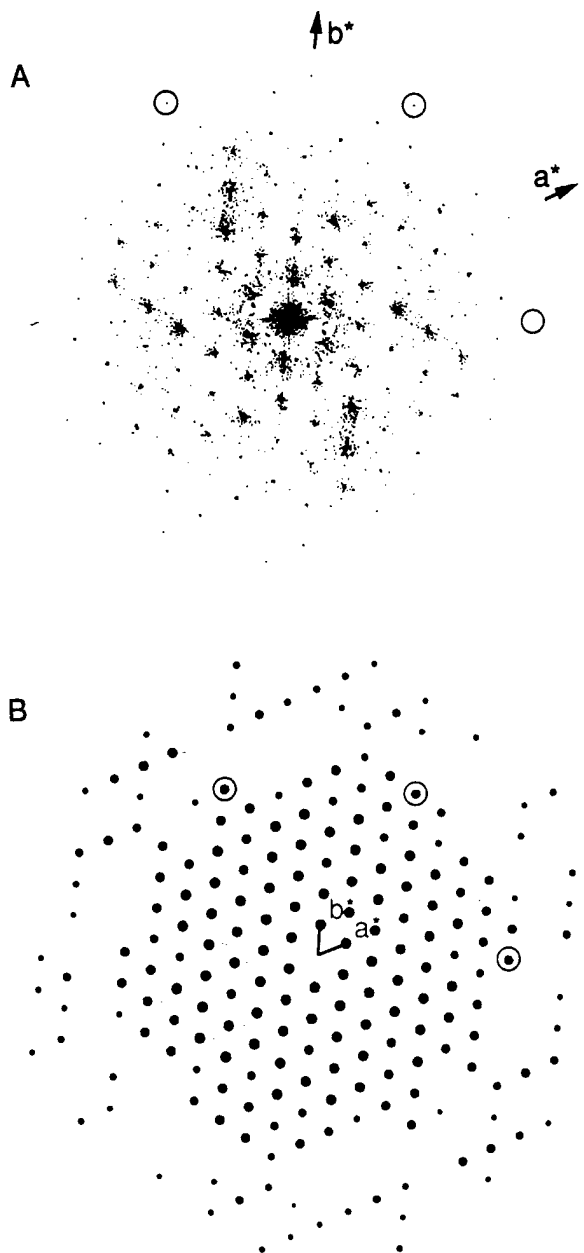


FIG. 2. (A) Computed diffraction pattern corrected for lattice distortions (Henderson *et al.*, 1986). The directions of the reciprocal lattice vectors a^* and b^* are shown. $a^* = 135 \text{ \AA}^{-1}$, $b^* = 139 \text{ \AA}^{-1}$, $\gamma^* = 60^\circ$. The highest resolution reflections apparent to the eye are circled. These are the 2,5, the 7,-3, and the 6,-6 at $\sim \frac{1}{22} \text{ \AA}^{-1}$ resolution. (B) "IQ" plot from same data. Size of filled circle reflects signal-to-noise ratio of spot at lattice position. Spot size ranges from largest ($IQ = 1$, $s:n > 7:1$) to smallest ($IQ = 4$, $s:n = 2.5:1$). Circled spots are same as in A.

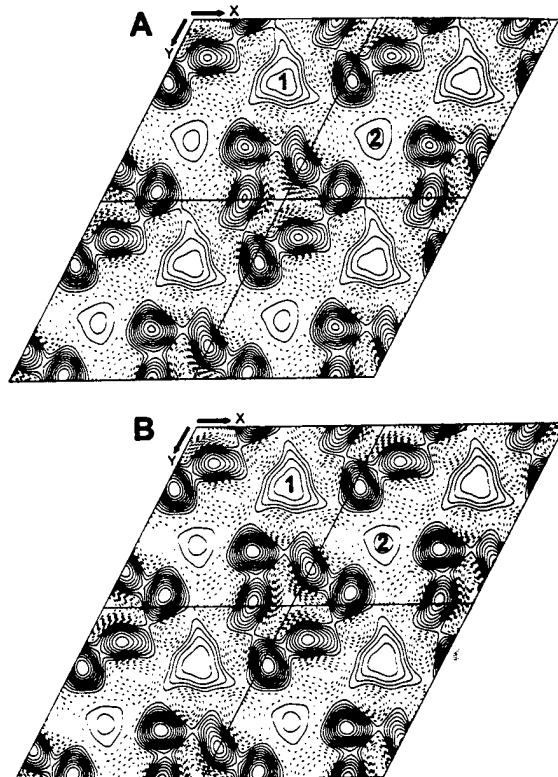


FIG. 3. Projection density maps calculated using noise-filtered Fourier coefficients merged from eight untilted images. Unbroken contours represent densities greater than the mean of the image. Each rhomboid represents one unit cell. (A) Projection map assuming no symmetry constraints (P1). (B) Projection density map calculated assuming P3 symmetry.

better transfer from the air-water interface will allow us to improve the resolution of the map.

DISCUSSION

The impetus for structural studies of the 900-kDa complex is that although its components have been well characterized, their stoichiometry and structural organization have not. While an initial investigation of the complex in negative stain yielded no structural information, the lipid-layer technique resulted in the crystals presented in this work. To make sense of the resultant projection map we will try to relate it to what little structural information is available.

The electron micrographs presented in Figs. 1B and 1C show that the structure of a monomeric complex is a central triangular density surrounded by radiating densities. These features are more clearly seen in the projection map of the complex (Figs. 3A and 3B), where they appear as a central triangle, composed of six densities, surrounded by two smaller, triangular densities, labeled "1" and "2." We believe that the less dense structures labeled 1

and 2 in Fig. 3A may be the radiating densities surrounding the incorporated monomers seen in Fig. 1B. Although we know which densities are found within the unit cell, we cannot define the molecular boundary of the complex with certainty. Thus in a single noncrystallized complex, densities 1 and 2 might be adjacent to one another on one side of the central triangle or at opposite ends of the central triangle.

It has previously been shown by sedimentation ultracentrifugation and diffusion constant measurements that the BoNTA-HA has a molecular frictional ratio (f/f_0) of 1.76 (Putnam *et al.*, 1948). From this value it was determined that the complex is a prolate ellipsoid with a molecular weight of 900 kDa. Results obtained from dynamic light scattering indicate that the radius is 110 Å and the molecular weight of the complex is 1200 kDa (Chen *et al.*, 1997b), assuming that the complex is spherical. Since the molecular weight calculated by dynamic light scattering is based on the hydrodynamic radius, and this is calculated on the assumption that the molecule is a sphere, deviations from a spherical shape will overestimate the calculated molecular weight. Based on the discrepancy between calculated molecular weights, it can be inferred that the complex is not spherical but elongated with a major axis of 220 Å.

An approximation of a protein's molecular weight based on its image in projection can be made by assuming the protein to be a sphere with a density of 1.3 g/cm³ (Cantor and Schimmel, 1980). This approximation works quite well on published maps such as the 133-kDa tetanus toxin (Robinson *et al.*, 1988) and the 117-kDa HIV-1 reverse transcriptase (Kubalec *et al.*, 1994). A 900-kDa spherical protein would have a diameter of 130 Å, fitting nicely into the unit cell but bearing no resemblance to the projection map, which consists of six central densities and two projecting triangular densities, 1 and 2 (Figs. 3A and 3B). Applying this approximation to the six central circular densities, and assuming each individual diameter is 40 Å, gives a total mass of 250 kDa, which falls short of the 900-kDa molecular weight. A better approximation is to consider the six central densities as cylinders instead of spheres. Stretching these densities into cylinders to bring the total mass to 900 kDa requires them to be 100 to 150 Å high. Since the two projecting triangular densities (1 and 2) contribute mass to the complex, then the height of the cylinders should be approximately 100 Å.

We have included both the *P*1 and the *P*3 structures (Figs. 3A and 3B) in this study. Although our projection map shows threefold symmetry, there is no biochemical evidence that BoNTA-HA is trimeric. Additionally, it is implausible that the unit cell

contains three 900-kDa protein complexes. Thus, we leave open the possibility that a higher resolution structure may show a reduced degree of symmetry. To reconcile the biochemical data with the electron microscopy, we propose the following model: The 900-kDa BoNTA-HA complex is composed of six cylinders approximately 40 Å in diameter by 100 Å high. These are arranged in a triangular pattern 130 Å on each side and hollow in the middle. Six smaller structures project radially 110 Å from the center of the triangle (yielding a 220-Å diameter in the plane of the projection map). Verification of this structure will require the generation of a higher resolution map both in projection and as a three-dimensional reconstruction.

We gratefully acknowledge Drs. Kenneth Downing and Robert Glaeser for many helpful discussions on electron microscopy and image processing. We also thank Dr. Bibhuti DasGupta and Bill Tepp for their generosity in supplying BoNTA-HA. This work was supported by the National Institutes of Health (Grants GM51487 and GM36884) and the Office of Health and Environmental Research, U.S. Department of Energy (under Contract DE-AC03-76F00098).

REFERENCES

- Amos, L. A., Henderson, R., and Unwin, P. N. T. (1982) Three-dimensional structure determination by electron microscopy of two dimensional crystals, *Prog. Biophys. Mol. Biol.* **39**, 183–231.
- Boroff, D. A., Nyberg, S., and Hoglund, S. (1972) Electron microscopy of the toxin and hemagglutinin of type A *Clostridium botulinum*, *Infect. Immun.* **6**(6), 1003–1007.
- Cantor, C. R., and Schimmel, P. R. (1980) Biophysical Chemistry, Part 1, The Conformation of Biological Macromolecules, pp. 115–116, Freeman, New York.
- Chen, F., Kuziemko, G. M., Amersdorfer, P., Wong, C., Marks, J. D., and Stevens, R. C. (1997) Antibody mapping to domains of botulinum neurotoxin serotype A in the complexed and uncomplexed forms, *Infect. Immun.* **65**(5), 1626–1630.
- Chen, F., Kuziemko, G. M., and Stevens, R. C. Submitted for publication.
- Crowther, R. A., Henderson, R., and Smith, J. M. (1996) MRC image processing programs, *J. Struct. Biol.* **116**, 9–16.
- Darst, S. A., Ahlers, M., Meller, P. H., Kubalek, E. W., Blankenburg, R., Ribi, H. O., Ringsdorf, H., and Kornberg, R. D. (1991) Two-dimensional crystals of streptavidin on biotinylated lipid layers and their interaction with biotinylated macromolecules, *Biophys. J.* **59**, 387–396.
- Darst, S. A., Ribi, H. O., Pierce, D. W., and Kornberg, R. D. (1988) Two-dimensional crystals of *Escherichia coli* RNA polymerase holoenzyme on positively charged lipid layers, *J. Mol. Biol.* **203**, 269–273.
- DasGupta, B. R. (1980) Electrophoretic analysis of clostridium botulinum types A and B hemagglutinins, *Can. J. Microbiol.* **26**, 992–997.
- DasGupta, B. R., and Boroff, D. A. (1968) Separation of toxin and hemagglutinin from crystalline toxin of *Clostridium botulinum* type A by anion exchange chromatography and determination of their dimensions by gel filtration, *J. Biol. Chem.* **243**(5), 1065–1072.
- DasGupta, B. R., and Sugiyama, H. (1977) Inhibition of Clos-

- tridium botulinum types A and B by sugars, *Can. J. Microbiol.* **23**, 1257–1260.
- Hayashi, T., McMahon, H., Yamasaki, S., Binz, T., Hata, Y., Südhof, T. C., and Niemann, H. (1994) Synaptic vesicle membrane fusion complex: Action of clostridial neurotoxins on assembly, *EMBO J.* **13**, 5051–5061.
- Henderson, R., Baldwin, J. M., Downing, K. H., Lepault, J., and Zemlin, F. (1986) Structure of purple membrane from *Halobacterium halobium*: Recording, measurement and evaluation of electron micrographs at 3.5 Å resolution, *Ultramicroscopy* **19**, 147–178.
- Kubalek, E. W., LeGrice, S. F. J., and Brown, P. O. (1994) Two-dimensional crystallization of histidine-tagged, HIV-1 reverse transcriptase promoted by a novel nickel-chelating lipid, *J. Struct. Biol.* **113**, 117–123.
- Moberg, L. J., and Sugiyama, H. (1978) Affinity chromatography purification of type A botulinum neurotoxin from crystalline toxic complex, *Appl. Environ. Microbiol.* **35**, 878–880.
- Morgan, D. G., DasGupta, B. R., Stubbs, B., and Robinson, J. P. (1989) Two dimensional crystals of botulinum toxin, serotype B, Proceedings of the Annual Meeting of the Electron Microscopy Society of America, pp. 1034–1035.
- Mosser, G., and Brisson, A. (1991) Conditions of two-dimensional crystallization of cholera toxin B-subunit on lipid films containing ganglioside GM1, *J. Struct. Biol.* **106**, 191–198.
- Putnam, F. W., Lamanna, C., and Sharp, D. G. (1948) Physicochemical properties of crystalline *Clostridium botulinum* type A toxin, *J. Biol. Chem.* **176**, 401–412.
- Robinson, J. P., Schmid, M. F., Morgan, D. G., and Chiu, W. (1988) Three-dimensional structural analysis of tetanus toxin by electron crystallography, *J. Mol. Biol.* **200**, 367–375.
- Simpson, L. L. (1980) Kinetic studies on the interaction between botulinum toxin type A and the cholinergic neuromuscular junction, *J. Pharmacol. Exp.* **212**, 16–21.
- Schmid, M. F., Robinson, J. P., and DasGupta, B. R. (1993) Direct visualization of botulinum neurotoxin-induced channels in phospholipid vesicles, *Nature* **364**, 827–830.
- Sugiyama, H. (1980) *Clostridium botulinum* neurotoxin, *Microbiol. Rev.* **44**, 419–448.
- Sugiyama, H., Moberg, L. J., and Messer, S. L. (1977) Improved procedure for crystallization of *Clostridium botulinum* type A toxic complexes, *Appl. Environ. Microbiol.* **33**(4), 963–966.
- Uzgiris, E. E., and Kornberg, R. D. (1983) Two-dimensional crystallization technique for imaging macromolecules, with application to antigen–antibody–complement complexes, *Nature* **301**, 125–129.

Recombinant Expression and Purification of the Botulinum Neurotoxin Type A Translocation Domain

D. Borden Lacy and Raymond C. Stevens¹

Department of Chemistry, University of California, Berkeley, California 94720

Received April 29, 1997, and in revised form June 9, 1997

Botulinum neurotoxin type A in its fully activated form exists as a dichain protein consisting of a 50-kDa light chain and a 100-kDa heavy chain linked by a disulfide bond (B. R. DasGupta and H. Sugiyama, *Biochem. Biophys. Res. Commun.* 48, 108–112, 1972). The protein can be further subdivided into three functional domains: a catalytic domain corresponding to the light chain, a translocation domain associated with the N-terminal half of the heavy chain, and a binding domain as the C-terminal half. To facilitate further structural and functional studies on the mechanism of toxin translocation, we report here the recombinant *Escherichia coli* expression and purification of the isolated translocation domain with a yield of 1 mg pure protein per 1 g cell paste. Circular dichroism, enzyme-linked immunosorbent assays, and preliminary crystallization experiments verify proper protein folding. This reagent should serve as a key tool in elucidating the mechanism of translocation and in determining how the catalytic domain, a large 50-kDa metalloprotease, is delivered to the cytosol. © 1997 Academic Press

Botulinum neurotoxin serotype A (BoNT/A)² is one of seven antigenically distinct proteins produced from strains of *Clostridium botulinum*. These serotypes (designated types A–G) are the causative agents of bot-

ulism, a potentially fatal condition of neuromuscular paralysis (2). The seven types of BoNT along with tetanus toxin comprise the clostridial toxin family. Comparison of the clostridial toxins to the better-characterized diphtheria toxin (DT) shows some important similarities. Both the clostridial toxins and DT are synthesized as a single chain and then posttranslationally nicked to form a dichain molecule held together by a disulfide bond. Their toxicity is believed to be a result of three functional domains (Fig. 1a shows BoNT/A) acting in a three-step mechanism to bind, enter, and catalyze a specific reaction within the cell. The idea that BoNT shares this three-step model of toxicity was first proposed by Simpson (3) and has since been supplemented with further experimental evidence and analogies to DT. The first step involves a binding interaction between the 50-kDa binding domain and a cell surface receptor on the presynaptic membrane (4). BoNT is thought to be internalized into an endosome via receptor-mediated endocytosis. The acidic pH of the endosome is believed to then cause a conformational change [best characterized for DT (5, 6)] in the 50-kDa translocation domain which allows it to interact with the endosomal membrane and form a channel (7, 8). The 50-kDa catalytic domain is translocated across the membrane, released from its disulfide linkage, and left free in the cytosol. The catalytic domain of each BoNT serotype is a zinc-dependent endopeptidase which targets specific sequences of proteins involved in vesicle docking and membrane fusion. BoNT/A's cleavage of a peptide bond in SNAP-25 (synaptosomal-associated protein of 25-kDa) (9) results in inhibition of acetylcholine release from the axon and, ultimately, paralysis (10).

Of particular interest is the proposed role of the BoNT translocation domain in the delivery of the catalytic domain to the cytosol: specifically, (i) the nature of the conformational change at acidic pH, (ii) the molecular mechanism of insertion, and (iii) the role the translocation domain plays—active or passive—in getting the 50-kDa catalytic domain into the cytosol.

¹ To whom correspondence should be addressed. Fax: (510) 643-9290.

² Abbreviations used: BoNT/A, botulinum neurotoxin type A; BoNT, botulinum neurotoxin; DT, diphtheria toxin; Tris, tris(hydroxymethyl)aminomethane; ECL, enhanced chemiluminescence; IPTG, isopropyl β-D-thiogalactopyranoside; PCR, polymerase chain reaction; EDTA, ethylenediaminetetraacetic acid; BoNT-trans, botulinum neurotoxin translocation domain; CD, circular dichroism; ELISA, enzyme-linked immunosorbent assay; PBS, phosphate-buffered saline; scFv, single-chain variable fragment; Fc, constant fragment; SDS-PAGE, sodium dodecyl sulfate-polyacrylamide gel electrophoresis; PE, *Pseudomonas* exotoxin A.

A great deal of insight into the phenomenon of translocation has come from studies done on diphtheria toxin, particularly since the elucidation of the atomic coordinates by X-ray crystallography (11). Using biochemical studies, researchers have used this structural information to assess the roles that both secondary structural elements and individual amino acids play in the translocation event (12–16).

In contrast, very little information about translocation is available for the clostridial toxins. While comparisons between toxin families have been useful in the initial understanding of BoNT, significant differences exist. Most notably, DT is a 58-kDa protein while BoNT is 150 kDa. The enormous size of BoNT relative to DT and all other toxins makes it uniquely interesting, especially in the context of cellular transport. Sequence comparisons indicate that when aligned to BoNT/A, the other serotypes and tetanus toxin have 55 to 66% homology. The translocation domains share a slightly higher homology of 60 to 70%. We, therefore, have pursued BoNT/A as a model system for studying translocation of the clostridial toxins.

As a first step in this investigation, the isolated translocation domain of BoNT/A has been cloned into a recombinant *Escherichia coli* overexpression system. This is the first report of translocation domain expression for botulinum neurotoxin along with initial biophysical characterization. Constructs were prepared both with and without cysteines and with silent mutations to improve homogeneity. Given the partial membrane–protein character of the domain, a detailed description of the purification is presented as well as preliminary structural experiments.

EXPERIMENTAL PROCEDURES

Materials. All buffer components and reagents were purchased from Sigma unless otherwise specified: Tris (Fisher Scientific), enhanced chemiluminescence (ECL) reagents (Amersham), DNase (Boehringer-Mannheim), silver-staining solutions (Bio-Rad), and isopropyl β -D-thiogalactopyranoside (IPTG) (Diagnostic Chemicals, Inc.). Restriction endonucleases were obtained from New England Biolabs, Inc. and used as directed by the supplier. T4 DNA ligase, T4 polymerase, and T4 polynucleotide kinase were obtained from Pharmacia Biotech, Inc. Additionally, Pharmacia supplied the chelating Sepharose fast flow resin and the reagents for fluorescence dideoxy sequencing that accompany their automated laser fluorescent (A.L.F.) DNA sequencer. The oligonucleotides for the polymerase chain reaction (PCR) were purchased from Genset, while the oligonucleotides for site-directed mutagenesis and sequencing were synthesized in-house on an Applied Biosystems 392 RNA/DNA synthesizer. Fluorescent primers were prepared with FluorePrime, a fluorescein amidite, also from Pharmacia.

Bacterial strains. *E. coli* strain DH5 α F' was used in the cloning procedures, *E. coli* strain CJ236 was used for mutagenesis, and *E. coli* strain BL21(DE3)pLysS was used for protein overexpression.

Construction of pET-23a/BoNT/A-trans. Plasmid DNA used for cloning and sequencing was prepared through either the alkaline lysis method (17) or with a kit supplied by QIAGEN. DNA encoding the BoNT/A catalytic and translocation domains was isolated from genomic DNA (18) by PCR and cloned into a pUC119 vector with a C-terminal myc epitope tag (GAACAAAAACTC-ATCTCAGAAGAGGATCTGAATGGGGCCGCA). This construct was prepared as a linear strand template for PCR to amplify just the translocation domain. Oligonucleotides were designed against the translocation domain and C-terminal myc epitope tag to include two unique restriction sites. The forward primer introduced a *Nde*I site at the 5' end of the gene (GAAAAAGGG-AAGGGACATATGGCATTAAATGATTATGTATCA-AAGTTAATAATTGG) and the reverse primer (GAAA-GAAAGAGGGGGCTCGAGTGCAGCCCCATTCA-GATCCTC) extended from the myc epitope tag to include a *Xho*I site. PCR products were gel-purified and extracted using the QIAGEN gel extraction kit. Following resuspension in TE (10 mM Tris, 1 mM EDTA, pH 8.0), the DNA was ligated into a pGEMT vector (Promega) by A/T overlaps and sequenced to check for correct PCR amplification. The DNA was then digested with *Nde*I and *Xho*I and ligated into the pET-23a vector (Novagen). The pET-23a *Xho*I site is followed by six histidine residues and the stop codon.

Site-directed mutagenesis. The pET-23a/BoNT/A-trans plasmid was transformed into a CJ236 dut[−] ung[−] strain of *E. coli*. Site-directed mutagenesis was performed using standard protocols for manipulating single-stranded uracil-containing DNA (17). The oligo for the silent mutations (GCCTAAAAACATAGCCGCTT-CGGTCGCTTATTAACTTCTTAC) took advantage of the degeneracy of the genetic code to eliminate the internal Shine–Dalgarno sequence. Two additional oligos were designed to replace the cysteines with alanines: (CAAGTCCCATTGTTAACCTTGATGGCCA-GATCATTTAATGCC) annealed around C454 and (CCATAAGGGATCATAGAGTTCATGAGATAAGAA-ACGCTAGCTTGATTCAAAAA) for C791. These two oligos were annealed and extended simultaneously to produce the double mutant.

Expression and purification of the translocation domain. Expression of the BoNT/A-trans domain was under the control of the T7 polymerase promoter in pET-23a. Initially, expression was done in 1-liter shaker flasks containing LB/carb/CAP [Luria-Bertani medium (17) containing 50 μ g/mL carbenicillin and 34 μ g/mL chloramphenicol]. The medium was inoculated with a single colony of BL21(DE3)pLysS carrying the

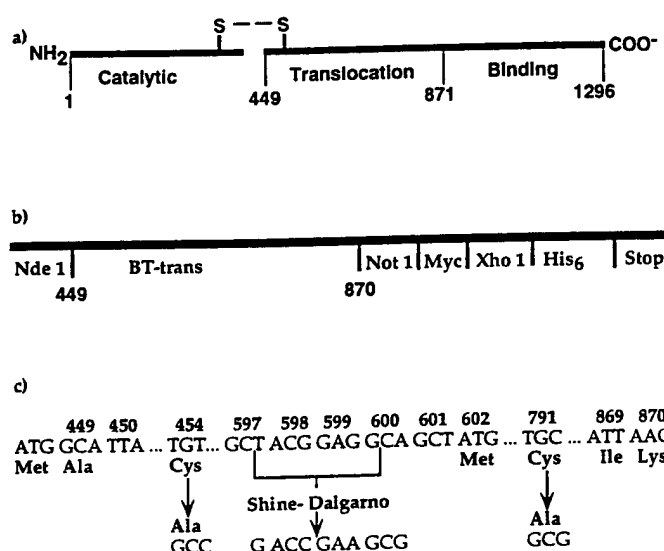


FIG. 1. BoNT/A-translocation domain constructs in pET23a. (a) The three functional domains of BoNT/A. (b) The original PCR product was cloned into pET-23a using *Nde*I and *Xho*I. (c) Site-directed mutagenesis was used to convert cysteines to alanines and to introduce silent mutations in the internal Shine-Dalgarno sequence.

desired plasmid, incubated with shaking at 37°C, and, at an OD = 0.6, induced with 1 mM IPTG. In later experiments, the cells were grown in a 200-liter fermentor with all reagents scaled up proportionally. Starting with 60 g of cell paste, the bacterial pellet was resuspended in 30 mL of binding buffer (500 mM NaCl, 5 mM imidazole, 0.3 mM methionine, and 20 mM

TABLE 1
Purification Summary

Purification step	Volume (mL)	Total protein (mg)
Detergent solubilization	30	ND
Metal affinity column	7.5	60

Note. The data were obtained from purification of the BoNT/A translocation domain from 60 g of cell paste as described under Experimental Procedures, using 10 mL of Pharmacia metal chelating resin.

Tris, pH 7.9). Protease inhibitors were added to final concentrations of 0.12 mg/mL phenylmethylsulfonyl fluoride (PMSF), 6.7 µg/mL pepstatin A, and 6.7 µg/mL leupeptin. Additionally, 200 µL of 1 M MgCl₂ and small amounts of DNase were added. Cells were lysed using a French press and the soluble and insoluble portions were separated by centrifugation. The pellet was washed with 30 mL binding buffer in the presence of 1 mL 0.5 M EDTA and recentrifuged prior to resuspension in a total volume of 30 mL binding buffer in 1% *n*-lauroyl sarcosine. Following centrifugation, the supernatant was filtered and further purified using metal affinity chromatography. A column packed with metal chelating resin was charged with either 50 mM NiSO₄ or CuSO₄. The column was pre-equilibrated with the binding buffer plus 1% sarcosyl solution be-

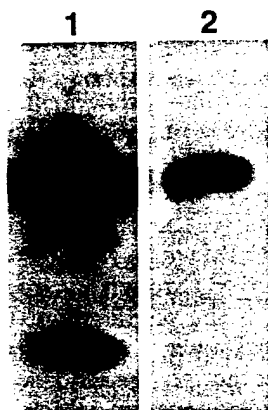


FIG. 2. Western blotting to confirm protein identity. SDS-PAGE was followed by transfer to nitrocellulose, sequential incubation with anti-Myc and anti-mouse horseradish peroxidase antibodies, and detection by ECL. Lane 1 contains 30 µg of protein and shows the translocation domain with lower molecular weight proteolysis and cotranslational contaminants. Lane 2 contains 2 µg of protein and shows just the BoNT/A translocation domain after steps had been taken to avoid the contaminants.

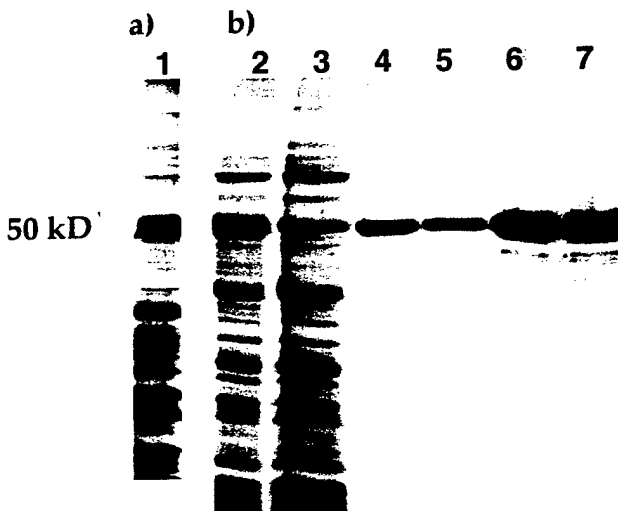


FIG. 3. SDS-PAGE to assess expression and purity of BoNT/A-trans. Electrophoresis was performed on a 10% acrylamide gel under reducing conditions with 30 µg of protein per lane. Protein bands were visualized by silver staining. Lanes 1 through 6 show the purification of the BoNT/A-trans (with all mutations incorporated) by metal affinity chromatography. Lane 1 shows what was loaded on the column, lane 2 represents the flowthrough, and lanes 3–6 show the purified protein after elution with 500 mM imidazole.

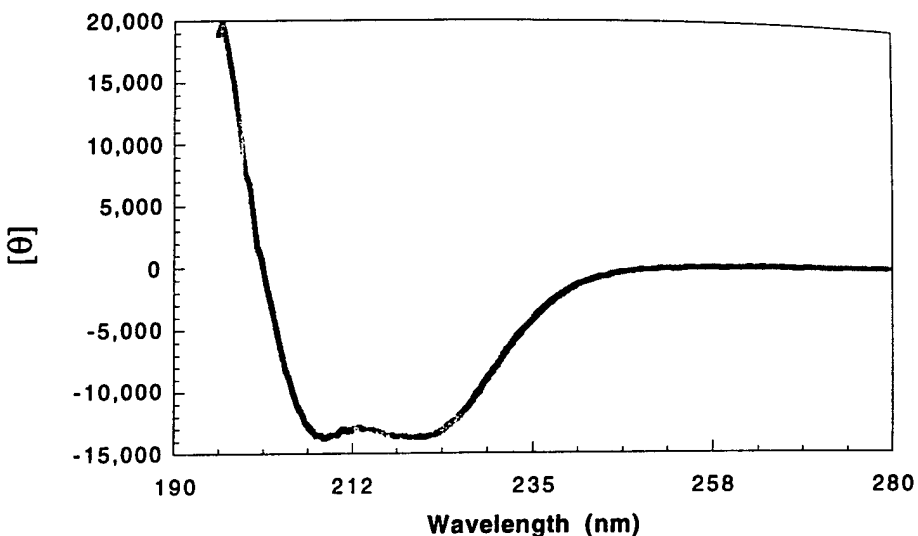


FIG. 4. Far-UV CD spectrum of the BoNT/A-translocation domain. A wavelength scan was taken at 25°C using a 1-cm path-length strain-free cuvette (BoNT/A-trans at 30 µg/mL, 5 mM potassium phosphate, pH 7.0, 5 mM KCl).

fore loading the protein. Following an extended wash step, the protein was eluted off the column by increasing the imidazole concentration to 500 mM.

Circular dichroism (CD). All CD spectra were obtained on an Aviv 62DS spectropolarimeter with a Peltier temperature-controlled sample holder and a 1-cm pathlength cuvette. Potassium phosphate buffers were prepared at pH 3, 6, 7, and 8. Potassium acetate was used as the buffer at pH 4 and 5.

Enzyme-linked immunosorbent assay (ELISA). Microtiter plates (Falcon 3912) were incubated with 50 µL of the translocation domain at 10 µg/mL in PBS (25 mM NaH₂PO₄, 125 mM NaCl, pH 7.0) at 4°C overnight. After washing once with PBS, wells were incubated with 50 µL bacterial supernatant containing native E-tagged single-chain variable fragment (scFv). Antibodies were detected using an anti-E-tag antibody (1 mg/mL) (Pharmacia), followed by peroxidase-conjugated anti-mouse Fc antibody (Sigma), and 2,2'-azinobis(3-ethylbenzthiazoline sulfonic acid) as substrate as described (19).

Crystal growth. Initial crystals were found from an incomplete factorial grid (20) using Crystal Screens I and II (Hampton Research). Crystals were grown at 4 and 25°C by the hanging drop vapor diffusion method from a starting protein concentration of 7.8 mg/mL.

Sequence homology. Sequence homology between the clostridial toxins was determined by the BLAST algorithm (21) to align sequences in the SwissProt database.

RESULTS AND DISCUSSION

Construction of a BoNT/A-trans overexpression system and related mutations. Primers were designed to

isolate the translocation domain as residues 449–870 (Fig. 1a) as determined in the complete amino acid sequence of the holotoxin (22). This construct's sequence differs from the target sequence by an N-terminal methionine to start translation, a C-terminal Myc epitope tag to facilitate detection by Western blot analysis, and a C-terminal polyhistidine tag to enable purification by metal affinity chromatography (Fig. 1b). The initial construct contains two cysteines which do not form a disulfide bond in the native protein since the N-terminal cysteine is known to form the disulfide bridge with the catalytic domain. While the initial cysteine-containing construct was shown to overexpress, unwanted inter- or intramolecular disulfides were prevented by replacing the two cysteines with alanines. This construct, BoNT/A-trans (C454A, C791A), was prepared by site-directed mutagenesis, verified by sequencing, and shown to express in similar yields to the original construct. The protein identity was verified by Western blot analysis (Fig. 2, lane 1). Here, the upper 50-kDa band corresponds to the translocation domain. The lower band at 40 kDa was a result of proteolytic cleavage and was removed through the incorporation of protease inhibitors in the purification. Interestingly, the lower band at 30 kDa was a result of an internal methionine codon located six bases downstream from a Shine–Dalgarno sequence in which only one of eight bases differed from the canonical sequence (Fig. 1c). This cotranslational contaminant was eliminated by introducing silent mutations in the internal Shine–Dalgarno sequence by site-directed mutagenesis. Specifically, the codons for Ala 597, Thr 598, Glu 599, and Ala 600 were changed to degenerate alternatives. These changes were again, verified by sequencing, and

new Western blot analysis showed the complete elimination of this contaminant (Fig. 2, lane 2), thereby dramatically improving the homogeneity of the sample.

Purification of the BoNT/A-translocation domain. The protein was expressed to the insoluble portion of the cell. After experimenting with a number of salts, denaturants, and detergents, 1% *n*-lauroyl sarcosine, a zwitterionic detergent, was found to be the most effective means of solubilizing the protein. The resolubilized protein was then further purified by metal affinity chromatography (Table 1). The sample (Fig. 3, lanes 3–6) is believed to be greater than 95% pure as assessed by Coomassie and silver stain gel electrophoresis with serial dilutions of protein. This expression and purification protocol yields 1 mg pure protein for every 1 g of cell paste. The translocation domain is folded and stable in solution as shown by CD, ELISA, and crystallization experiments.

CD spectropolarimetry. Since the recombinant protein was isolated from the insoluble fraction, it is especially important to determine if the protein is folded. Far-UV CD spectropolarimetry of the recombinant protein showed a spectrum indicative of secondary structure as evidenced by the minima at 208 and 222 nm (Fig. 4). Similar wavelength scans were taken in 1-unit pH increments from 3 to 8. Two different buffering agents were required to achieve the optimal pK_a 's. It was interesting to observe that the spectra at pH 3, 6, 7, and 8 were identical. Unfortunately, spectra could not be attained at pH 4 and 5, as the protein was insoluble under these conditions. This 4–5 pH range is also the pH range of the endosome when the putative conformational change occurs. The calculated *pI* of the protein domain is 3.6. While it is not surprising that the protein would become more insoluble as it rearranges itself to interact with the membrane, further efforts will be made to find conditions where these changes can be monitored by biophysical techniques.

ELISA. Further evidence in support of a properly folded structure comes from work in mapping antibodies binding the holotoxin to the individual domains (23). Of the 40 scFv's that mapped to the holotoxin, three mapped exclusively to the translocation domain. ELISAs on these three antibodies were performed on protein purified as described above and on the same protein after heat denaturation. The denatured protein showed no signal by ELISA, possibly indicating that the antibodies recognize a conformational epitope as opposed to a linear one.

Preliminary crystallization results. The final piece of evidence in favor of structured protein was that the protein has been shown to crystallize in the presence of 100 mM magnesium formate, 100 mM Tris, pH 8.5, and 1 mM sodium azide (Fig. 5). While not yet of diffraction quality, the ability to grow crystals indicates a



FIG. 5. Preliminary crystallization of the BoNT/A-translocation domain. The protein was concentrated to 7.8 mg/mL and crystallized in the presence of 100 mM magnesium formate. Crystals were grown at 4°C in 2 days by the hanging drop method.

specific molecular packing arrangement unlikely for denatured proteins. Crystals were confirmed to be protein by staining with methylene blue and by analysis of crystals by SDS-PAGE.

CONCLUSION

The BoNT/A translocation domain is part of a soluble holoprotein that does not become activated until it enters the endosome. Once inside the endosome, the low pH is believed to induce conformational changes in the translocation domain that allow it to merge with the endosomal cell membrane and carry the 50-kDa catalytic domain to the cytosol. Once in the cytosol, the protease is able to perform the final function of the toxin, the inhibition of synaptic vesicle fusion resulting in nerve paralysis. Efforts to understand the basic mechanism of toxin translocation events have been undertaken in a number of systems, including DT (12–

16), *Pseudomonas* exotoxin A (PE) (24), ricin (25), and shiga toxin (26). However, none of these other toxins carry such a large 50-kDa protein to the cytosol. The ability to produce the translocation domain in suitable amounts provides the opportunity to study the translocation event in BoNT/A. Since botulinum neurotoxin is able to carry such a large protein to the cytosol, the translocation domain could possibly be harnessed to deliver other large proteins to their targets within the cytosol, analogous to immunotoxin and protein design strategies pursued previously with DT and PE (27–29). A further understanding of the translocation mechanism will greatly aid in this endeavor.

ACKNOWLEDGMENTS

This work was supported in part by the U. S. Army Medical Research and Development Command (DAMD17-93-C-3118), a NSF predoctoral fellowship (B.L.), and a NSF Young Investigator Award (R.C.S.). We thank Carl Chen for the initial genomic DNA cloning and Flora Chen for performing the ELISA experiments.

REFERENCES

- DasGupta, B. R., and Sugiyama, H. (1972) A common subunit structure in *Clostridium botulinum* type A, B and E toxins. *Biochem. Biophys. Res. Commun.* **48**, 108–112.
- Sugiyama, H. (1980) *Clostridium botulinum* neurotoxin. *Microbiol. Rev.* **44**, 419–448.
- Simpson, L. L. (1980) Kinetic studies on the interaction between botulinum toxin type A and the cholinergic neuromuscular junction. *J. Pharmacol. Exp. Ther.* **212**, 16–21.
- Dolly, J. O., Black, J., Williams, R. S., and Melling, J. (1984) Acceptors for botulinum neurotoxin reside on motor nerve terminals and mediate its internalization. *Nature* **307**, 457–460.
- Blewitt, M. G., Chung, L. A., and London, E. (1985) Effect of pH on the conformation of diphtheria toxin and its implications for membrane penetration. *Biochemistry* **24**, 5458–5464.
- Dumont, M. E., and Richards, F. M. (1988) The pH-dependent conformational change of diphtheria toxin. *J. Biol. Chem.* **263**, 2087–2097.
- Hoch, D. H., Romero-Mira, M., Ehrlich, B. E., Finkelstein, A., DasGupta, B. R., and Simpson, L. L. (1985) Channels formed by botulinum, tetanus, and diphtheria toxins in planar lipid bilayers: Relevance to translocation of proteins across membranes. *Proc. Natl. Acad. Sci. USA* **82**, 1692–1696.
- Schmid, M. F., Robinson, J. P., and DasGupta, B. R. (1993) Direct visualization of botulinum neurotoxin-induced channels in phospholipid vesicles. *Nature* **364**, 827–830.
- Blasi, J., Chapman, E. R., Link, E., Binz, T., Yamasaki, S., De Camilli, P., Südhof, T. C., Niemann, H., and Janh, R. (1993) Botulinum neurotoxin A selectively cleaves the synaptic protein SNAP-25. *Nature* **365**, 160–163.
- Burgen, A. S. V., Dickens, F., and Zalman, L. J. (1949) The action of botulinum toxin on the neuromuscular junction. *J. Physiol. (London)* **109**, 10–24.
- Choe, S., Bennett, M. J., Fujii, G., Curmi, P. M. G., Kantardjieff, K. A., Collier, R. J., and Eisenberg, D. (1992) The crystal structure of diphtheria toxin. *Nature* **357**, 216–222.
- Johnson, V. G., Nicholls, P. J., Habig, W. H., and Youle, R. J., (1993) The role of Proline 345 in diphtheria toxin translocation. *J. Biol. Chem.* **268**, 3514–3519.
- Madshus, I. H. (1994) The N-terminal α -helix of fragment B of diphtheria toxin promotes translocation of fragment A into the cytoplasm of eukaryotic cells. *J. Biol. Chem.* **269**, 17723–17729.
- vanderSpek, J., Cassidy, D., Genbauffe, F., Huynh, P. D., and Murphy, J. R. (1994) An intact transmembrane helix 9 is essential for the efficient delivery of the diphtheria toxin catalytic domain to the cytosol of target cells. *J. Biol. Chem.* **269**, 21455–21459.
- Silverman, J. A., Mindell, J. A., Finkelstein, A., Shen, W. H., and Collier, R. J. (1994) Mutational analysis of the helical hairpin region of diphtheria toxin transmembrane domain. *J. Biol. Chem.* **269**, 22524–22532.
- Zhan, H., Oh, K. J., Shin, Y.-K., Hubbell, W. L., and Collier, R. J. (1995) Interaction of the isolated transmembrane domain of diphtheria toxin with membranes. *Biochemistry* **34**, 4856–4863.
- Maniatis, T., Fritsch, E. F., and Sambrook, J. (1982) "Molecular Cloning: A Laboratory Manual," Cold Spring Harbor Laboratory Press, Cold Spring Harbor, NY.
- Betley, M. J., Somers, E., and DasGupta, B. R. (1989) Characterization of botulinum type A neurotoxin gene: Delineation of the N-terminal encoding region. *Biochem. Biophys. Res. Commun.* **162**, 1388–1395.
- Schier, R., Bye, J., Apell, G., McCall, A., Adams, G. P., Malmquist, M., Weiner, L. M., and Marks, J. D. (1996) Isolation of high-affinity monomeric human anti-c-erbB-2 single chain Fv using affinity-driven selection. *J. Mol. Biol.* **255**, 28–43.
- Jancarik, J., and Kim, S. H. (1991) Sparse matrix sampling—A screening method for crystallization of proteins. *J. Appl. Crystallogr.* **24**, 409–411.
- Altschul, S. F., Gish, W., Miller, W., Myers, E. W., and Lipman, D. J. (1990) Basic local alignment search tool. *J. Mol. Biol.* **215**, 403–410.
- Binz, T., Kurazono, H., Wille, M., Frevert, J., Wernars, K., and Niemann, H. (1990) The complete sequence of botulinum neurotoxin type A and comparison with other clostridial neurotoxins. *J. Biol. Chem.* **265**, 9153–9158.
- Chen, F., Kuziemko, G. M., Amersdorfer, P., Wong, C., Marks, J. D., and Stevens, R. C. (1997) Antibody mapping to domains of botulinum neurotoxin serotype A in the complexed and uncomplexed forms. *Infect. Immun.* **65**, 1626–1630.
- Theuer, C. P., Buchner, J., FitzGerald, D., and Pastan, I. (1993) The N-terminal region of the 37-kDa translocated fragment of *Pseudomonas* exotoxin A aborts translocation by promoting its own export after microsomal membrane insertion. *Proc. Natl. Acad. Sci. USA* **90**, 7774–7778.
- Beaumelle, B., Alami, M., and Hopkins, C. R. (1993) ATP-dependent translocation of ricin across the membrane of purified endosomes. *J. Biol. Chem.* **268**, 23661–23669.
- Sandvig, K., Garred, Prydz, K., Kozlov, J. V., Hansen, S. H., and van Deurs, B. (1992) Retrograde transport of endocytosed shiga toxin to the endoplasmic reticulum. *Nature* **358**, 510–512.
- Stenmark, H., Moskaug, J., Madshus, I. H., Sandvig, K., and Olsnes, S. (1991) Peptides fused to the amino-terminal end of diphtheria toxin are translocated to the cytosol. *J. Cell Biol.* **113**, 1025–1032.
- Madshus, I. H., Olsnes, S., and Stenmark, H. (1992) Membrane translocation of diphtheria toxin carrying passenger protein domains. *Infect. Immun.* **60**, 3296–3302.
- Prior, T. I., FitzGerald, D. J., and Pastan, I. (1992) Translocation mediated by domain II of *Pseudomonas* exotoxin A: Transport of barnase into the cytosol. *Biochemistry* **31**, 3555–3559.

Biophysical Characterization of the Stability of the 150-Kilodalton Botulinum Toxin, the Nontoxic Component, and the 900-Kilodalton Botulinum Toxin Complex Species

FLORA CHEN,¹ GEOFFREY M. KUZIEMKO,^{2,3} AND RAYMOND C. STEVENS^{2,3*}

Graduate Group in Biophysics¹ and Department of Chemistry,² University of California,
and Material Sciences Division, Lawrence Berkeley National
Laboratory,³ Berkeley, California 94720

Received 2 February 1998/Returned for modification 16 February 1998/Accepted 4 March 1998

Botulinum neurotoxin serotype A is initially released from the bacterium *Clostridium botulinum* as a stable 900-kDa complex. The serotype A 900-kDa complex is one of the forms of the toxin being used as a therapeutic agent for the treatment of various neuromuscular disorders. Previous experiments have demonstrated that the 900-kDa complex form of the toxin protects the toxin from the harsh conditions of the gastrointestinal tract. To provide molecular level details of the stability and equilibrium of the 900-kDa complex, the nontoxic component, and the toxic (botulinum neurotoxin) component, the three species have been investigated with a series of biophysical techniques at the molecular level (dynamic light scattering, proteolysis, circular dichroism, pH incubations, and agglutination assays). These experiments were conducted under harsh conditions which mimic those found along the gastrointestinal tract. Separately, exposure to denaturing and proteolytic conditions degrades both the botulinum neurotoxin and the nontoxic component. In the 900-kDa complex, the botulinum neurotoxin is protected during exposure to the gastrointestinal environment and the nontoxic component is slightly modified. Surprisingly, the toxin protects the ability of the nontoxic component to agglutinate erythrocytes. Contrary to previous reports, the purified 900-kDa complex did not have agglutination ability until after exposure to the proteolytic conditions. These experiments provide new evidence and detail for the theory that the nontoxic component and the toxic component protect one another during exposure to harsh conditions, and a molecular model is presented for the passage of the toxin through the gastrointestinal tract.

Botulinum neurotoxin is secreted by the anaerobic bacterium *Clostridium botulinum* as one of seven serotypes, classified A through G (35). The different serotypes proteolytically cleave specific proteins involved in synaptic vesicle docking that are necessary for cellular communication at the neuromuscular junction (12). Serotype A can be purified as a 900-kDa complex (BoNTA-HA) consisting of a toxic component (BoNTA [botulinum neurotoxin serotype A]) and a nontoxic component (HA [hemagglutinin]) (5–7). Studies involving relative oral toxicities (26, 33), intestinal absorption (34), and comparison to tetanus toxin (31) have indicated that the complex, not the botulinum toxin alone, is responsible for the extremely low amount of botulinum neurotoxin required in botulism poisoning.

The most common mechanism of botulism poisoning is through oral ingestion of the complex, which is found in food contaminated with *C. botulinum*. Ingested spores of the bacteria may also colonize and produce toxin in the intestinal tracts of infants, resulting in infant botulism (36). Previous experiments have demonstrated that the 900-kDa complex protects the toxin during its exposure to harsh conditions. Ohishi and coworkers (26) have demonstrated that the 900-kDa complex has a 360-fold-higher oral toxicity in rats than the 150-kDa botulinum neurotoxin component alone. Most proteins are broken down into peptides and amino acids in the stomach and small intestine during the process of digestion (2). However, the 900-kDa complex enters the stomach and withstands the

acidic (pH 2) gastric juice containing the protease pepsin. The complex then enters the small intestine, where it encounters several more proteases (trypsin, chymotrypsin, and carboxypeptidase) that function at pH 7 to 8. Despite these harsh denaturing and proteolytic conditions, active botulinum neurotoxin (13, 22) and nontoxic component (34) can be detected in the lymph and circulatory systems.

The botulinum neurotoxin is comprised of a C-terminal 100-kDa heavy chain and an N-terminal 50-kDa light chain linked by a disulfide bond. From C terminus to N terminus, the protein can be further divided into three 50-kDa functional domains (3, 4, 18)—binding, translocation, and catalytic—which allow the protein to bind a cell surface receptor, pass across the membrane (29), and cleave a protein involved in synaptic vesicle docking (12), respectively. The nontoxic component is composed of several protein subunits and can be separated into nontoxic agglutinating proteins (14, 17, 32) and nontoxic nonagglutinating proteins (11, 14). Several subcomponents of the nontoxic component have been characterized. One of the nontoxic nonagglutinating proteins is a single peptide of 120 kDa and has been sequenced (11). The molecular weights of the subcomponents of the nontoxic agglutinating portion have also been determined (14, 32). However, the physiological role and molecular organization of the nontoxic component are not well understood. In addition, many of the studies of toxin exposure to harsh conditions have been conducted with crude cell supernatant. To understand the stability and equilibrium of the botulinum neurotoxin complex and its separated components at the molecular level, we conducted a series of biophysical experiments using pure preparations of botulinum neurotoxin, botulinum neurotoxin complex, and the nontoxic agglutinating portion.

* Corresponding author. Mailing address: Department of Chemistry, University of California, Berkeley, CA 94720. Phone: (510) 643-8285. Fax: (510) 643-9290. E-mail: stevens@adrenaline.berkeley.edu.

MATERIALS AND METHODS

Purification of proteins. For all experiments, proteins were obtained as ammonium sulfate precipitates and were purified by ion-exchange chromatography as previously described (5).

Light scattering. The hydrodynamic radius, estimated molecular weight, and polydispersity of protein samples were determined by using a Dynapro-801 dynamic light scattering instrument (Protein Solutions, Charlottesville, Va.). Samples of botulinum neurotoxin (0.18 mg/ml), nontoxic component (0.20 mg/ml), and 900-kDa complex (0.22 mg/ml) were incubated for 30 min at 4°C over a range of pHs in 10 mM buffers containing 100 mM sodium chloride. Buffers were citric acid (pH 1 to 5) (citric acid has three pK_as at 25°C; pK₁ = 3.128, pK₂ = 4.761, and pK₃ = 6.396), bis-Tris [bis(2-hydroxyethyl)imino-tris(hydroxymethyl) methane; pH 6], HEPES (pH 7 to 8), and CHES [2-(N-cyclohexylamino)ethanesulfonic acid] (pH 9 to 10). Individual samples were recorded for at least 5 min, during which 12 to 13 data points were taken and then analyzed by using a monomodal fitting program. The polydispersity served as the deviation of the size distribution based on the mean hydrodynamic radius of each sample. Experiments were performed in triplicate.

Test for pH effects. Protein samples were incubated at the appropriate pH for 48 h at 4°C. Protein samples were subjected to sodium dodecyl sulfate-polyacrylamide gel electrophoresis (SDS-PAGE) on a 12% polyacrylamide gel, and the bands were visualized with silver stain (10).

Proteolysis. Proteins were incubated at various pHs and with several protease mixtures. Each protein sample contained 2 ml of protein (0.42 mg/ml) in dialysis tubing with a 50-kDa pore size. Dialysis tubing containing the protein sample was placed into the appropriate protease mixture. The mixture was incubated with gentle stirring for 2 h at 37°C. Pepsin incubations were performed with 0.4 mg of pepsin per ml in 10 mM hydrochloric acid (pH 2). Intestinal cocktail consisted of trypsin (0.02 mg/ml), chymotrypsin (0.03 mg/ml), and carboxypeptidase A (0.02 mg/ml) in 50 mM sodium bicarbonate-100 mM sodium chloride buffer (pH 8). Protease concentrations used were chosen based on reported values (15, 16), though the physiological protease concentration depends on the feeding state of the organism. After incubation, proteases were quenched with 0.5 ml of pepstatin (1 mg/ml) or phenylmethylsulfonyl fluoride (17.4 mg/ml) and 1 ml of 0.5 M EDTA. Proteins were also exposed to incubation of pepsin followed by intestinal cocktail or incubation at pH 2 followed by intestinal cocktail. Gels were 12% polyacrylamide, and protein bands were visualized with silver stain (10).

Circular dichroism. Circular dichroic spectra were gathered on a model J-600 spectropolarimeter (Jasco, Easton, Md.) at 37 and 25°C. The bandwidth used was 1 nm, and the step resolution was 2 nm. Four scans of each sample were made, using a time constant of 1 s and a scan rate of 50 nm/min. The cell volume was approximately 1 ml, with a path length of 0.1 cm. The cell was jacketed for temperature adjustment and controlled by using a water bath. Proteins at a concentration of 0.025 mg/ml were dialyzed extensively in their buffers before being examined on the spectropolarimeter. The pH 6 and pH 8 buffers were 100 mM sodium phosphate containing 100 mM sodium chloride. The pH 2 buffer was 60 mM hydrochloric acid-potassium chloride buffer containing 100 mM NaCl. No appreciable difference in signal was observed at 37 and 25°C; thus, only 37°C data are shown.

ELISA. Botulinum neurotoxin (0.01 mg/ml) was incubated in pepsin (0.4 mg/ml) and intestinal cocktail (see above) for 2 h at 37°C. The concentration of substrate protein used was the minimum amount of protein necessary to give strong enzyme-linked immunosorbent assay (ELISA) signal. Using single-chain variable fragments of mouse or of human monoclonal antibodies, ELISAs were performed on proteolyzed samples as described by Chen et al. (5).

Surface plasmon resonance. Binding of botulinum neurotoxin and 900-kDa complex to lipid was monitored by using surface plasmon resonance on a BIACore 2000 (Biosensor, Piscataway, N.J.). Botulinum neurotoxin (84 to 1,300 nM) or 900-kDa complex (52 to 832.5 nM) was injected over a lipid monolayer containing 1-palmitoyl-2-oleoyl-sn-glycero-3-phosphocholine (POPC). The lipid monolayer was formed by incubating a solution of POPC liposomes (2 mg/ml) on a BIACore sensorchip (type HPA) overnight in a moist environment. Liposomes were made by sonicating a solution of POPC in a buffer of 10 mM Tris (pH 7.0) containing 100 mM sodium chloride and 2 mM sodium azide. The experiments were performed at a flow rate of 40 µl/min for 20 min in running buffer of 10 mM Tris (pH 7.0) containing 100 mM sodium chloride and 2 mM sodium azide.

Sugar binding. Agglutination assays were performed as previously described (20). Erythrocytes (RBC) from rabbits were washed twice with saline (68 mM sodium citrate, 146 mM sodium chloride [pH 7.4]), spun at 4,000 × g, and diluted to 0.5% for each assay. Protein solution (0.5 ml) at twice the desired concentration was added to a disposable semimicrocuvette. Then 0.5 ml of the 0.5% RBC was added to the protein, resulting in the desired protein concentration and a 0.25% RBC solution. The mixture was incubated at 37°C for 2 h, and the transmittance was measured at 405 nm in a Shimadzu UV-160 spectrophotometer. The saline control contained 0.25% RBC incubated in saline for 2 h at 37°C. Each sample was performed in triplicate. The 900-kDa complex and nontoxic component were also proteolyzed and then used in an agglutination assay. The saline control was subtracted from the values for the other samples. The agglutination ability of the unproteolyzed HA was scaled to a value of 100. The agglutination abilities of the other samples represent their percent transmittances relative to the percent transmittance by unproteolyzed HA. Previous

reports (20) show that the 900-kDa BoNTA-HA complex is capable of agglutination at lower temperatures. When we performed the agglutination assay at a lower temperature (12°C), we observed that the complex showed an increased ability to agglutinate RBC, consistent with the literature but not physiologically relevant.

RESULTS AND DISCUSSION

Light scattering. Dynamic light scattering was used to determine the aggregation state and stability of the three species under a variety of conditions simulating the environments in the gastrointestinal tract. This technique measures the diffusion coefficient of particles in solution, allowing a radius and estimated molecular weight to be calculated. A molecular weight calculated to be higher than expected indicates a deviation from a spherical shape. This deviation may be due to nonspherical species, denatured protein, or the presence of large aggregates of many proteins. The distribution of particle sizes is indicated by the polydispersity value. A polydispersity of zero signifies that there is only one particle size in solution. A large polydispersity value indicates the presence of different-size particles in solution. Examination of the radii of the three molecular species between pH 1 and 10 yielded a number of intriguing results. From the hydrodynamic radii the corresponding molecular weights were calculated, assuming an approximate, spherical shape for the protein.

Between pH 10 and 4, the estimated molecular mass of BoNTA was determined to be approximately 150 kDa (Fig. 1A and D), corresponding to the expected molecular mass of a single BoNTA molecule (6). Upon incubation at pH 3 to 1, botulinum neurotoxin showed steadily higher values for molecular mass, from 150 to over 1,000 kDa, during the first 10 min in the corresponding buffer. The polydispersity also increased dramatically as the pH changed from 3 to 1. These higher values for polydispersity correlated with aggregation and acid-catalyzed degradation of the neurotoxin molecule. This result is consistent with botulinum neurotoxin retaining little toxicity at pH 3 to 1 (33). Examination of the nontoxic component at various pHs revealed behavior similar to that of the botulinum neurotoxin (Fig. 1B and D). The nontoxic component did not aggregate or disassemble between pH 10 and 5 and had an apparent estimated molecular mass of approximately 962 kDa. The molecular mass calculated by light scattering differs from that calculated by subtracting the molecular mass of the BoNTA from the molecular mass of the BoNTA-HA complex because the nontoxic component most likely is not spherical. Since the light scattering device calculates a molecular mass by a formula that assumes the protein is a sphere, deviations in sphericity will result in deviations in molecular mass. The nontoxic component aggregated, disassembled, or denatured when the pH dropped from pH 5 to 4, corresponding to a sharp increase in the polydispersity between pH 5 (0%) and 4 (polydispersity/radius = 18.1%). Below pH 4, the nontoxic component increased in size to over 2,000 kDa. In contrast to the botulinum neurotoxin and the nontoxic component, the entire BoNTA-HA complex was most stable and monodisperse between pH 1 and 4 (Fig. 1C and D), correlating with the observation that the BoNTA-HA complex retains over 60% of its toxicity at low pH (33). Between pH 5 and 7, the complex reached its maximum size. Near neutral pH, the complex reached its maximum polydispersity. A similar high polydispersity was observed upon ultracentrifugation at pH 7.5 (37). Above pH 8, the complex appeared as a more polydisperse species, suggesting the presence of more than one species in solution probably due to disassociation of the complex into the toxic and nontoxic components. This idea of dissociation at basic pH is supported by the procedure for

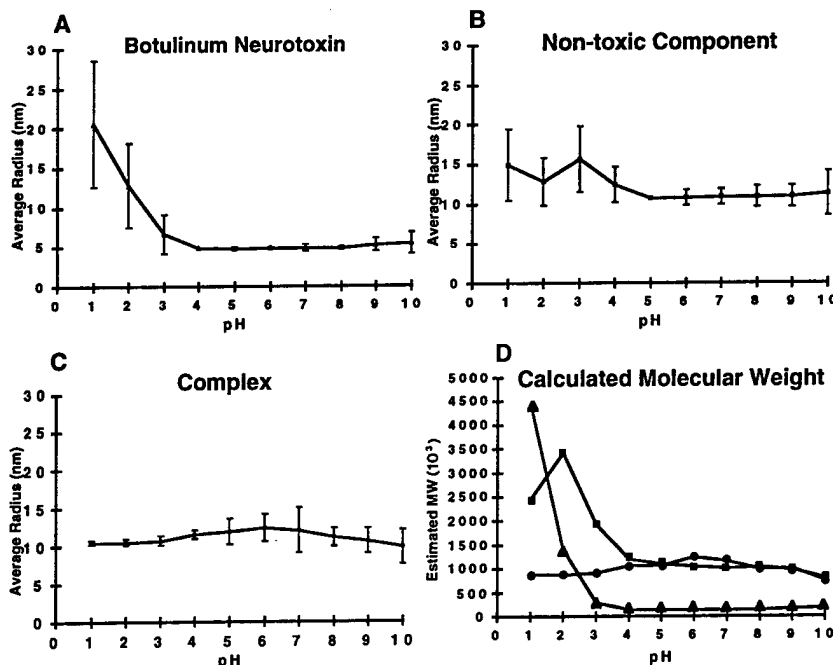


FIG. 1. Dynamic light scattering results, expressed as pH versus apparent radius and molecular weight of botulinum neurotoxin (A), nontoxic component (B), and 900-kDa complex (C) at various pHs. (D) Estimated molecular weights (MW) of botulinum neurotoxin (triangles), nontoxic component (squares), and 900-kDa complex (circles). The bar around each data point represents the average polydispersity value for three separate experiments. The polydispersity is the deviation of size distributions based on the mean radius measurement. Specimens containing aggregates or unfolded proteins have large polydispersity values.

purifying botulinum neurotoxin from the complex, since high pH is necessary for separation of toxic and nontoxic components (6, 7).

pH effects. The effect of pH on the neurotoxin's structural stability was examined by SDS-PAGE. A polyacrylamide gel of botulinum neurotoxin incubated at pH 2, 6, and 8 for 48 h indicated that the neurotoxin is susceptible to breakdown at pH 2 and 8 (Fig. 2). Table 1 shows that nonincubated neurotoxin runs as a 100-kDa heavy chain and a 50-kDa light chain. After 48 h of incubation at pH 6, we observed primarily the 100-kDa heavy chain and 50-kDa light chain of botulinum neurotoxin. A band at 150 kDa corresponded to a small quantity of unnickled neurotoxin. Although the 100- and 50-kDa bands predominated at pH 2 and 8, we observed a ladder of many lower-molecular-weight fragments. This fragmentation could be a result of acid-catalyzed hydrolysis, base-catalyzed hydrolysis, or proteolysis.

Proteolysis. Besides pH extremes, the other stresses that the 900-kDa complex must endure come from proteases. The effects of proteases on botulinum neurotoxin, nontoxic component, and 900-kDa complex were observed by performing protease incubations and assaying the results by gel electrophoresis (Table 1). Incubations consisted of pepsin at pH 2, intestinal cocktail (trypsin, chymotrypsin, carboxypeptidase) at pH 8, and pepsin at pH 2 followed by intestinal cocktail at pH 8. When incubated individually, both the neurotoxin and the nontoxic component were susceptible to all of the protease incubations (Table 1). In contrast, the 900-kDa complex demonstrated an amazing resistance to proteolysis. After incubation in pepsin at pH 2, the 900-kDa complex lost none of its bands. When the 900-kDa complex was incubated in intestinal cocktail, the 100- and 50-kDa bands of botulinum neurotoxin were proteolyzed along with the 120- and 106-kDa bands of the nontoxic component. However, incubating the 900-kDa complex in pepsin at pH 2 before exposing the complex to

intestinal cocktail inhibited the proteolysis of the bands corresponding to botulinum neurotoxin. The bands which have been previously shown to be responsible for agglutination (14, 19, 21, 35, and 52 kDa) (14, 32) remained intact according to our gel whereas the band previously shown to be nontoxic-nonagglutinating (11) was destroyed.

Thus, under conditions that simulate the path of the 900-kDa complex through the gastrointestinal tract, the nontoxic component protected botulinum neurotoxin from proteolysis. This protection of the neurotoxin could be due to exposure to pepsin or to acidic pH. To determine if the protection of botulinum neurotoxin was a result of low pH, we performed an incubation without pepsin at pH 2, followed by an intestinal cocktail incubation. With these conditions, we observed that low pH was sufficient for protecting the complexed botulinum neurotoxin from proteolysis (data not shown). This protection of the botulinum neurotoxin in the 900-kDa complex was also seen upon incubations in rat gastric juice (33).

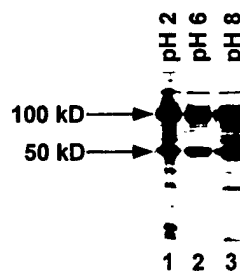


FIG. 2. SDS-PAGE of botulinum neurotoxin incubated at pH 2, 6, and 8. Arrows identify the heavy chain (100 kDa) and light chain (50 kDa) of botulinum neurotoxin. The band appearing at approximately 150 kDa is unnickled neurotoxin.

TABLE 1. Proteolysis and agglutination ability of BoNTA, nontoxic component (HA), and 900-kDa BoNTA-HA complex

Protein	Unproteolyzed			Pepsin (pH 2)			Intestinal cocktail (pH 8)			Sequental pepsin (pH 2)/ intestinal cocktail (pH 8)		
	No. of bands on 12% gel ^a	Aggluti- nation ^b	No. of bands on 12% gel	No. of bands on 12% gel	Aggluti- nation	No. of bands on 12% gel	No. of bands on 12% gel	Aggluti- nation	No. of bands on 12% gel	Aggluti- nation	No. of bands on 12% gel	
BoNTA	2 (50, 100)	4.4	2 (30, 25)	—	4 (40, 45, 50, 100)	—	0	—	—	—	—	
HA	7 (14, 19, 21, 35, 52, 106, 120)	100	7 (7, 14, 19, 21, 35, 52, 106, 120)	87.8	5 (14, 19, 21, 35, 52)	—	5 (14, 19, 21, 35, 52)	—	5 (14, 19, 21, 35, 52)	—	10.4	
BoNTA-HA complex	9 (14, 19, 21, 35, 50, 52, 100, 106, 120)	1	9 (14, 19, 21, 35, 50, 52, 100, 106, 120)	9.4	5 (14, 19, 21, 35, 52)	—	7 (14, 19, 21, 35, 50, 52, 100)	—	7 (14, 19, 21, 35, 50, 52, 100)	—	37.9	

^a Numbers in parentheses indicate sizes (in kilodaltons) of bands appearing on 12% acrylamide gels under denaturing and reducing conditions.

^b Percent transmittance by the protein relative to the percent transmittance by unproteolyzed HA, which was scaled to 100. Saline control value was subtracted from the sample values before scaling to the unproteolyzed HA value. —, no activity.

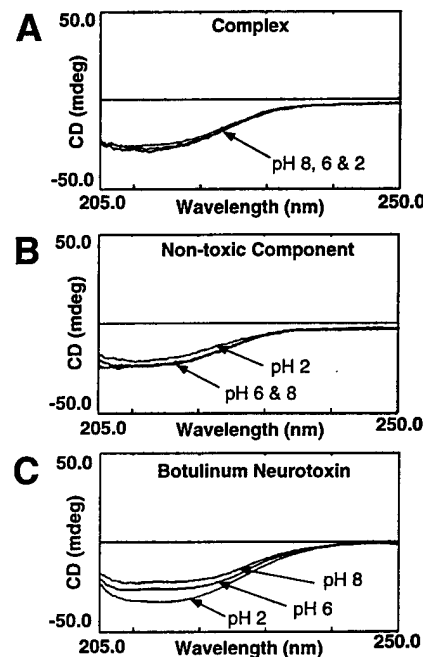


FIG. 3. Circular dichroism (CD) spectra of the 900-kDa complex at pH 8 (top), pH 6 (middle), and pH 2 (bottom) (A), the nontoxic component at pH 2 (top), pH 6 (middle), and pH 8 (bottom) (B), and botulinum neurotoxin at pH 8 (top), pH 6 (middle), and pH 2 (bottom) (C).

Circular dichroism. Circular dichroic spectra of the botulinum neurotoxin, the nontoxic component, and the complex were taken at 37 and 25°C to determine the effects of pH on the structure and stability of the proteins. Temperature appeared not to have an effect on the spectra. At pH 2, 6, and 8, the 900-kDa complex shows little change in secondary structure (Fig. 3A). Thus, the increased protease resistance of the 900-kDa complex, upon exposure to pH 2, did not result from a visible conformational change in the secondary structure. When the nontoxic component was studied at pH 6 and 8, it likewise showed minor change in secondary structure (Fig. 3B). Upon exposure to pH 2, the nontoxic component showed a slight decrease in helicity. This loss of secondary structure is not large enough to indicate that the nontoxic component significantly unfolds. Since individual nontoxic components do not unfold, an increase in hydrodynamic radius, which corresponds to an increase in the size of the particle being observed, likely results from the aggregation of multiple nontoxic components. This aggregation explains the size increase of the nontoxic component observed by light scattering (Fig. 1B).

The greatest change in secondary structure occurred with the botulinum neurotoxin. Circular dichroism spectroscopy on botulinum toxin and its separated components at pH 8.1 have shown that approximately 70% of the amino acid residues exist in an ordered structure (30). Previous reports of circular dichroic data from pH 9 to 6 revealed a slight increase in alpha helicity (8). Our results for botulinum neurotoxin show an increase in helicity on moving from pH 8 to 6 (Fig. 3C). However, a larger increase in helicity occurred on moving from pH 6 to 2. This increase in helicity may be due to a conformational change in the translocation domain of the neurotoxin, which is known to form pores upon exposure to acidic pH (4). If the neurotoxin increases its helicity at pH 2, producing more secondary structure, then botulinum neurotoxin does not unfold in an acidic environment. Consequently, the huge increase in

hydrodynamic radius indicated by light scattering (Fig. 1A) is most likely caused by a conformational change in the molecular structure, followed by oligomerization or aggregation of the botulinum neurotoxin.

ELISA and surface plasmon resonance. The nontoxic component appears to prevent the vulnerable regions of the botulinum neurotoxin from protease attack, acid hydrolysis, and aggregation at low pH. Epitope mapping suggests that in the 900-kDa complex, the nontoxic component covers a large portion of the binding domain of botulinum neurotoxin (5). Previous experiments have shown that the binding domain is highly susceptible to trypsin cleavage (28). Therefore, the nontoxic component may play an important role in protecting the binding domain in the gastrointestinal tract. Furthermore, ELISA performed on botulinum neurotoxin after pepsin and intestinal proteolysis showed that antibodies no longer bind to it, suggesting that cleavage, denaturation, or both have occurred. In addition to being highly susceptible to proteolysis, botulinum neurotoxin appears to stick strongly and irreversibly to lipid monolayers such as POPC, a lipid commonly found in membranes of cells lining the gastrointestinal tract (9). Using surface plasmon resonance, we found that botulinum neurotoxin injected over POPC monolayers adsorbed strongly whereas the 900-kDa complex did not. Similarly, unless the toxic component was in its complexed form, it would probably adhere to lipid membranes along the gastrointestinal tract. Additional evidence for the association of botulinum neurotoxin with phospholipids has been seen by several researchers (17, 24, 25, 27). Thus, without the nontoxic component for protection, botulinum neurotoxin might never leave the gastrointestinal tract but instead be digested like most other proteins.

Sugar binding. The only known ability of the nontoxic component is its capacity to bind certain sugars (1). Upon binding these sugars, the nontoxic component is able to agglutinate, or clump together, cells (19). Whether this property aids the neurotoxin in reaching its target is under investigation. The clumping of RBC was monitored with agglutination assays (Table 1). Previous work has shown that the 14-, 19-, 21-, 35-, and 52-kDa bands are primarily responsible for agglutination (14, 32). Unproteolyzed nontoxic component containing these five bands was able to agglutinate RBC at 37°C (Table 1). After proteolysis by pepsin (pH 2), the nontoxic component experienced a slight decrease in agglutination ability (Table 1). Upon exposure to sequential protease incubations, the nontoxic component showed the largest decrease in the ability to agglutinate RBC (Table 1). This decrease appears to correlate with the loss of the 120- and 106-kDa bands (Table 1). The 106-kDa band was shown to be a proteolyzed portion of the 120-kDa band (14). Therefore, the 120-kDa band appears to be necessary for the nontoxic component to maintain optimal agglutination ability by protecting the other proteins but is not directly involved in agglutination. When unproteolyzed or exposed to pepsin, the complex showed a low ability to agglutinate (Table 1). Upon exposure to a sequential pepsin and intestinal cocktail incubation, the complex increased its ability to agglutinate RBC (Table 1). The sequentially proteolyzed complex contains the 14-, 19-, 21-, 35-, and 52-kDa bands plus the 100- and 50-kDa bands corresponding to botulinum neurotoxin (Table 1). Thus, the presence of botulinum neurotoxin appears to protect the ability of the complex to agglutinate after a sequential protease incubation.

These experiments indicate that in order for the nontoxic component to maintain optimal agglutination activity, it must be part of the 900-kDa complex while traveling through the gastrointestinal tract. After exposure to the conditions simulating the gastrointestinal tract, the 900-kDa complex appears

to be modified so that the agglutination ability is activated. We propose that the 900-kDa complex may then interact with sugars on RBC and release the 150-kDa neurotoxin into the circulatory system. Although further experiments are necessary, experiments in which the 900-kDa complex was incubated with RBC that were subsequently pelleted by centrifugation and washed in saline solution (0.85% NaCl) showed that the neurotoxin was released and remained active in the supernatant (21). In addition, the neurotoxin has been shown to separate from the nontoxic component when the latter is bound to a sugar affinity column (23) and eluted with buffers at basic pH and ionic strength.

The 900-kDa complex form of botulinum neurotoxin is necessary for the delivery of botulinum neurotoxin in its most potent form. Using purified material and examining the results of the different toxin species at the molecular level, we have provided further evidence that the neurotoxin must exist in the 900-kDa complex to maintain its activity in conditions mimicking the environment of the gastrointestinal tract. In addition, a synergistic partnership between botulinum neurotoxin and the nontoxic component in which the nontoxic portion preserves the toxic ability of the toxic portion and the toxic portion protects the agglutinating ability of the nontoxic component seems to exist. In the 900-kDa complex, the neurotoxin and nontoxic component protect each other from pH extremes and gastrointestinal proteases. In contrast, when separated and exposed to simulated digestive conditions, each component is degraded. Although the molecular mechanism of the neurotoxin's journey to the neuromuscular junction is still unclear, these biophysical studies provide further evidence and detail as to the importance of the 900-kDa complex in the potent oral toxicity of botulinum neurotoxin.

ACKNOWLEDGMENTS

F. Chen and G. M. Kuziemko contributed equally to the work.

We thank B. R. DasGupta and Bill Tepp for generous supplies of botulinum neurotoxin, 900-kDa complex, and nontoxic component. We also thank the lab of Ignacio Tinoco, Jr., especially Barbara Dengler, for use of their circular dichroism spectropolarimeter.

This work was supported in part by the U.S. Army Medical Research and Development Command (DAMD17-93-C-3118), an NSF Young Investigator Award (R.C.S.), U.S. Department of Energy contract DE-AC03-76SF0098, and a National Institutes of Health predoctoral traineeship from the Neurobiology Division, University of California, Berkeley.

REFERENCES

- Balding, P., E. R. Gold, D. A. Boroff, and T. A. Roberts. 1973. Observations on receptor specific proteins. II. Haemagglutination and haemagglutination-inhibition reactions of Clostridial botulinum types A, C, D and E haemagglutinins. Immunology 25:773-782.
- Beck, W. S., K. F. Liem, and A. R. Simpson. 1991. Life, an introduction to biology, 3rd ed., p. 666-676. Harper Collins Publishers, Inc., New York, N.Y.
- Blasi, J., E. R. Chapman, E. Link, T. Binz, S. Yamasaki, P. De Camill, T. C. Südhof, H. Niemann, and R. Jahn. 1993. Botulinum neurotoxin A selectively cleaves the synaptic protein SNAP-25. Nature 365:160-163.
- Blaustein, R. O., W. J. Germann, A. Finkelstein, and B. R. DasGupta. 1987. The N-terminal half of the heavy chain of botulinum type A neurotoxin forms channels in planar phospholipid bilayers. FEBS Lett. 226:115-120.
- Chen, F., G. M. Kuziemko, P. Amersdorfer, C. Wong, J. D. Marks, and R. C. Stevens. 1997. Antibody mapping to domains of botulinum neurotoxin serotype A in the complexed and uncomplexed forms. Infect. Immun. 65: 1626-1630.
- DasGupta, B. R., and D. A. Boroff. 1968. Separation of toxin and hemagglutinin from crystalline toxin of *Clostridium botulinum* type A by anion exchange chromatography and determination of their dimensions by gel filtration. J. Biol. Chem. 243:1065-1072.
- DasGupta, B. R., D. A. Boroff, and E. Rothstein. 1966. Chromatographic fractionation of the crystalline toxin of *Clostridium botulinum* type A. Biochem. Biophys. Res. Commun. 22:750-756.
- Datta, A., and B. R. DasGupta. 1988. Circular dichroic and fluorescence

- spectroscopic study of the conformation of botulinum neurotoxin types A and E. *Mol. Cell. Biochem.* 79:153-159.
9. Dudeja, P. K., J. M. Harig, K. Ramaswamay, and T. A. Brasitus. 1989. Protein-lipid interaction in human small intestinal brush-border membranes. *Am. J. Physiol.* 257:G809-G817.
 10. Fling, S. P., and D. S. Gregerson. 1988. Peptide and protein molecular weight determination by electrophoresis using a high-molarity Tris buffer system without urea. *Anal. Biochem.* 155:83-88.
 11. Fujita, R., Y. Fujinaga, K. Inoue, H. Nakajima, H. Kumon, and K. Oguma. 1995. Molecular characterization of two forms of nontoxic-nonhemagglutinin components of *Clostridium botulinum* type A progenitor toxins. *FEBS Lett.* 376:41-44.
 12. Hayashi, T., H. McMahon, S. Yamasaki, T. Binz, Y. Hata, T. C. Südhof, and H. Niemann. 1994. Synaptic vesicle membrane fusion complex: action of clostridial neurotoxins on assembly. *EMBO J.* 2:5051-5061.
 13. Heckly, R. J., G. J. Hildebrand, and C. Lamanna. 1960. On the size of the toxic particle passing the intestinal barrier in botulism. *J. Exp. Med.* 111: 745-759.
 14. Inoue, K., Y. Fujinaga, T. Watanabe, T. Ohyama, K. Takeshi, K. Moriishi, H. Nakajima, K. Inoue, and K. Oguma. 1996. Molecular composition of *Clostridium botulinum* type A progenitor toxins. *Infect. Immun.* 64:1589-1594.
 15. Johnson, L. R. 1981. Physiology of the gastrointestinal tract, p. 625-627. Raven Press Books, Ltd., New York, N.Y.
 16. Johnson, L. R. 1981. Physiology of the gastrointestinal tract, p. 784-787. Raven Press Books, Ltd., New York, N.Y.
 17. Kamata, Y., Y. Kimura, and S. Kozaki. 1994. Involvement of phospholipids in the intoxication mechanism of botulinum neurotoxin. *Biochim. Biophys. Acta* 1199:65-68.
 18. Kozaki, S., A. Miki, Y. Kamata, T. Nagai, J. Ogasawara, and G. Sakaguchi. 1989. Immunological characterization of the papain-induced fragments of *Clostridium botulinum* type A neurotoxin and interaction of the fragments with brain synaptosomes. *Infect. Immun.* 57:2634-2639.
 19. Lamanna, C. 1948. Hemagglutination by botulinum toxin. *Proc. Soc. Exp. Biol. Med.* 69:332-336.
 20. Lowenthal, J. P., and C. Lamanna. 1951. Factors affecting the botulinum hemagglutination reaction, and the relationship between hemagglutinating activity and toxicity of toxin preparations. *Am. J. Hyg.* 54:342-353.
 21. Lowenthal, J. P., and C. Lamanna. 1953. Characterization of botulinum hemagglutination. *Am. J. Hyg.* 57:46-59.
 22. May, A. J., and B. C. Whaler. 1958. The absorption of *Clostridium botulinum* type A toxin from the alimentary canal. *Br. J. Exp. Pathol.* 39:307-316.
 23. Moberg, L. J., and H. Sugiyama. 1978. Affinity chromatography purification of type A botulinum neurotoxin from crystalline toxin complex. *Appl. Environ. Microbiol.* 35:878-880.
 24. Montecucco, C., G. Schiavo, Z. Gao, E. Bauerlein, P. Boquet, and B. R. DasGupta. 1988. Interaction of botulinum and tetanus toxins with the lipid bilayer surface. *Biochem. J.* 251:379-383.
 25. Montecucco, C., G. Schiavo, and B. R. DasGupta. 1989. Effect of pH on the interaction of botulinum neurotoxins A, B and E with liposomes. *Biochem. J.* 259:47-53.
 26. Ohishi, I., S. Sugii, and G. Sakaguchi. 1977. Oral toxicities of *Clostridium botulinum* in response to molecular size. *Infect. Immun.* 16:107-109.
 27. Schmid, M. F., J. P. Robinson, and B. R. DasGupta. 1993. Direct visualization of botulinum neurotoxin-induced channels in phospholipid vesicles. *Nature* 364:827-830.
 28. Shone, C. C., P. Hambleton, and J. Melling. 1985. Inactivation of *Clostridium botulinum* type A neurotoxin by trypsin and purification of two tryptic fragments. *Eur. J. Biochem.* 151:75-82.
 29. Simpson, L. L. 1980. Kinetic studies on the interaction between botulinum toxin type A and the cholinergic neuromuscular junction. *J. Pharmacol. Exp. Ther.* 212:16-21.
 30. Singh, B. R., and B. R. DasGupta. 1989. Structure of heavy and light chain subunits of type A botulinum neurotoxin analyzed by circular dichroism and fluorescence measurements. *Mol. Cell. Biochem.* 85:67-73.
 31. Singh, B. R., B. Li, and D. Read. 1995. Botulinum versus tetanus neurotoxins: why is botulinum neurotoxin but not tetanus neurotoxin a food poison? *Toxicology* 33:1541-1547.
 32. Somers, E., and B. R. DasGupta. 1991. *Clostridium botulinum* types A, B, C, and E produce proteins with or without hemagglutinating activity: do they share common amino acid sequences and genes? *J. Protein Chem.* 10:415-425.
 33. Sugii, S., I. Ohishi, and G. Sakaguchi. 1977. Correlation between oral toxicity and in vitro stability of *Clostridium botulinum* type A and B toxins of different molecular sizes. *Infect. Immun.* 16:910-914.
 34. Sugii, S., I. Ohishi, and G. Sakaguchi. 1977. Intestinal absorption of botulinum toxins of different molecular sizes in rats. *Infect. Immun.* 17:491-496.
 35. Sugiyama, H. 1980. *Clostridium botulinum* neurotoxin. *Microbiol. Rev.* 44: 419-448.
 36. Tacket, C. O., and M. A. Rogawski. 1989. Botulism, p. 354-356. In L. L. Simpson (ed.), *Botulinum neurotoxin and tetanus toxin*. Academic Press, Inc., San Diego, Calif.
 37. Wagman, J., and J. B. Bateman. 1953. Botulinum type A toxin: properties of a toxic dissociation product. *Arch. Biochem. Biophys.* 45:375-383.

Editor: J. T. Barbieri

Crystal Structure of Botulinum Neurotoxin Type A and Implications for Toxicity

D. Borden Lacy¹, William Tepp²,
Bibhuti R. DasGupta², and Raymond C. Stevens¹

¹Department of Chemistry and Ernest Orlando Lawrence Berkeley National Laboratory, University of California, Berkeley, CA 94720, USA. ²Department of Food Microbiology and Toxicology, University of Wisconsin, Madison, WI 53706, USA.

Correspondence should be addressed to R. C. S. e-mail:stevens@adrenaline.berkeley.edu

Botulinum neurotoxin type A (BoNT/A) is the potent disease agent in botulism, a potential biological weapon and an effective therapeutic drug for involuntary muscle disorders. The crystal structure of the entire 1285 amino acid dichain neurotoxin was determined at 3.2 Å resolution. The structure reveals that the translocation domain contains a central pair of 105 Å α -helices and a ~50 residue belt that wraps around the catalytic domain. This belt partially occludes a large channel leading to a buried, negative active site- a feature which calls for radically different inhibitor design strategies from those currently used. The fold of the translocation domain suggests a mechanism of pore formation different from other toxins. Lastly, the toxin appears as a hybrid of varied structural motifs and suggests a modular assembly of functional subunits to yield pathogenesis.

The clostridial neurotoxin family is composed of tetanus neurotoxin and seven serotypes of botulinum neurotoxin (BoNT/A - BoNT/G). Botulinum neurotoxin serotype A is synthesized in *Clostridium botulinum* as a ~150 kDa single chain protein (1296 amino acids). The toxin is post-translationally proteolyzed to form a 1285 amino acid dichain molecule in which the two chains, ~50 kDa and ~100 kDa, remain linked by a disulfide bond¹. The protein is composed of three ~50 kD functional domains where the catalytic function is confined to the ~50 kDa chain (residues 1 to 437), the translocation activity with the N-terminal half of the ~100 kDa chain (residues 448-872), and receptor binding with its C-terminal half (residues 873 to 1295)^{1,2}. The toxicity of BoNT is a result of a multi-step mechanism³. The neurotoxin binds to the pre-synaptic nerve endings of cholinergic neurons and enters by receptor-mediated endocytosis. Acidity in the endosome is believed to induce pore formation, which allows translocation of the catalytic domain into the cytosol. The zinc-dependent catalytic domain of the seven BoNT serotypes specifically cleaves one of three different SNARE proteins essential for synaptic vesicle fusion: synaptobrevin, syntaxin, or SNAP-25. This cleavage results in inhibition of acetylcholine secretion, ultimately leading to paralysis¹.

What remains unknown is how the highly homologous BoNT serotypes and tetanus derive specificity both for different receptors and their different SNARE protein targets. Furthermore, a number of questions surround the mechanism by which a soluble protein changes with acidic pH to one that can span a membrane and translocate a ~50 kD protein. We describe here the crystal structure of BoNT/A and then use this structural information to address some of these mechanistic questions.

Overall structure of botulinum neurotoxin type A

The crystal structure of BoNT/A was determined by multiple isomorphous replacement (MIR) using five heavy-atom derivatives (Table 1). Phases were further improved with solvent flattening to yield readily interpretable electron density maps (Fig. 1). The model, which includes 99% of the amino acids, was refined to 3.2 Å with an R value of 20.0% and an R_{free} value of

27.9%. The BoNT/A molecule is approximately 45 Å x 105 Å x 130 Å and shows a linear arrangement of the three functional domains with no contact between the catalytic and binding domains (Fig. 2). In general, the three functional domains are also structurally distinct. The exception is an unusual loop, or belt, from what has historically been considered part of the translocation domain, that wraps around the perimeter of the catalytic domain.

Receptor binding domain

The binding domain, overall 32 Å x 37 Å x 76 Å, appears as two distinct sub-domains roughly equal in size. Both sub-domains are predominantly composed of β-strands and are connected by one prominent α-helix. The N-terminal sub-domain has two seven-stranded β-sheets sandwiched together in a jelly roll motif with dimensions 32 Å x 37 Å x 38 Å. The C-terminal sub-domain has similar dimensions and adopts a modified β-trefoil fold with a six-stranded β-barrel next to the N-terminal jelly roll motif and a β-hairpin triplet capping the base of the domain. The entire binding domain tilts away from the long helical axis of the translocation domain such that there is no contact between the C-terminal sub-domain and the translocation domain and all of the surface loops are accessible for binding. The binding domain shares structural homology with the recently solved structure of the tetanus toxin binding domain⁴ with an rms deviation of 1.5 Å for 363 Cα positions (Fig. 3). The major differences appear in the loops of the C-terminal sub-domain, where the longer loop lengths in the tetanus toxin sub-domain account for the domain's slightly longer length in primary sequence.

The first step in the intoxication mechanism is a binding event between the binding domain and the pre-synaptic nerve ending. The interaction with BoNT/A is proposed to occur through both a polysialoganglioside (G_{D1b} or G_{T1b}) and a yet unidentified protein receptor^{5,6}. The putative ganglioside binding site for tetanus neurotoxin, as assessed by photoaffinity labelling⁷, is in a loop of the C-terminal sub-domain, and when overlayed with the BoNT/A holotoxin structure, is fully accessible. This could represent a general ganglioside binding site for all the clostridial neurotoxins. It is striking that both sub-domains have structural homology with

proteins known to interact with sugars as assessed using Dali⁸, a three-dimensional search algorithm, and its ranked output according to Z-score. (The Z-score is the strength of structural similarity in standard deviations over the expected where pairs with Z<2 are structurally dissimilar.) The top twelve proteins after tetanus toxin (Z=26.3) structurally similar to the N-terminal sub-domain are proteins known to interact with sugars (i.e. serum amyloid P (1sac-A, Z=12.8), β -glucanase (2ayh, Z=11.1), sialidase (1kit, Z=8.9), lectin (1led, Z=8.8)). Perhaps the most notable of these twelve are cryia (1ciy, Z=5.2) and insecticidal δ -endotoxin (1dlc, Z=4.8) which act by binding glycoproteins and creating leakage channels⁹. These toxins have binding domains structurally similar to the N-terminal sub-domain of BoNT/A but dramatically different pore-forming domains. A Dali search of the C-terminal sub-domain reveals more sugar binding proteins (basic fibroblast growth factor (1bfg, Z=9.1), agglutinin (1jly-A, Z=9.9)) and the toxin abrin (1abr-B, Z=8.8). Both abrin and the related ricin bind their targets through a β -trefoil binding domain. The appearance of different subsets of the same structural motifs in different toxins could suggest a mechanism of evolution in which stable functional domains are assembled as modular units giving rise to toxicity.

Pore-formation and translocation domain

Following cell surface binding and receptor-mediated endocytosis of the neurotoxin, an acid-induced conformational change in the neurotoxin's translocation domain is believed to allow the translocation domain to penetrate the endosome and form a pore. The membrane interaction and pore formation is thought to facilitate the passage of the catalytic domain across the membrane into the cytosol. The details of how the translocation domain changes conformation at acidic pH to form a pore and how it can allow for the passage of a 50 kDa catalytic domain across the endosomal membrane are the least understood aspects of the intoxication mechanism. To date, most investigations of the translocation event in BoNT have assumed a similarity to other pH dependent α -helical pore-forming proteins: diphtheria toxin, colicin A, δ -endotoxin,

pseudomonas exotoxin, and Bcl-x_L⁹⁻¹³. These proteins share a common structural motif in their pore forming domain^{13,14}, however this motif is not observed in the BoNT/A structure.

The translocation domain of BoNT/A wraps around the catalytic domain before forming its main body, a cylindrical shape with dimensions of 28 Å x 32 Å x 105 Å (Fig.2). The most salient feature of the translocation domain is a pair of α -helices 105 Å long corresponding to residues 685-827. While unusual, long pairs of α -helices have been observed recently in the structures of colicin Ia¹⁵ and the nucleotide exchange factor GrpE¹⁶. The helices, anti-parallel and amphipathic, twist around each other like a coiled coil but do not adhere to a strict heptad repeat. At both ends of this pair of helices, a shorter α -helix packs in parallel to the long helical axis. In addition, the domain has two strand-like sections which pack against the pair of α -helices in a parallel fashion. In an effort to identify the pore-forming segment of BoNT/A, the primary sequence was searched for predicted amphipathic helicity, and the candidate segment (residues 659-681) was shown to increase permeability of lipid bilayers¹⁷. The present structure, solved at neutral pH, shows that none of this putative transmembrane segment is helical and that, in fact, part of it appears to be in one of the two strand-like segments packing against the long α -helices. This could indicate an area which will undergo structural changes with pH. However, the residues most likely to titrate over this pH range are the two histidines in the translocation domain, which are located away from this region of the structure. His 551 and His 560 are located in a loop between the translocation domain belt and the main body of the translocation domain. This junction may play a role in exposing a hydrophobic segment of the protein or releasing the catalytic domain from the translocation domain. Regardless of the pore-forming segment location, it is clear that the translocation domain of BoNT/A is structurally distinct from the other pore-forming toxins. In fact, the long pair of α -helices with their triple helix bundles at either end bear more resemblance to the coiled coil viral proteins: HIV-1 gp41/GCN4, influenza hemagglutinin, and the MoMuLV TM fragment¹⁸⁻²⁰. These proteins do not translocate through pores but do have an acid-induced ability to undergo structural changes and penetrate membranes.

Catalytic domain

Either within the acidic endosome or upon exposure to the cytosol following translocation, the disulfide bond connecting the catalytic and translocation domains (Cys 429 to Cys 453) is reduced, and the catalytic domain is released into the cytoplasm. The catalytic domain, 55 Å x 55 Å x 62 Å, is a mixture of both α -helix and β -strand secondary structure, in agreement with secondary structure predictions.³⁶ The active site of the catalytic domain is buried 20-24 Å deep in the protein, has a negative surface charge, and is accessible by a channel, ~12 Å x 15 Å x 35 Å, (Fig. 4). In the dichain holotoxin, this channel is partially shielded from solvent by both the belt and the main body of the translocation domain.

The final mechanistic step in toxicity is the cleavage of a presynaptic protein by the BoNT zinc protease catalytic domain. The catalytic zinc atom represents the highest peak in the electron density maps and is visible in MIR maps contoured at 7.5 σ . Amino acids with side chains closest to the zinc include His 222, Glu 223, His 226, Glu 261, and Tyr 365 (Fig. 5). While the presence of His 222, Glu 223, and His 226 was anticipated¹, this structure identifies Glu 261 as the fourth ligand, and may help resolve uncertainty in tetanus toxin where either Glu 269 or Glu 270 had been implicated²¹. (Glu 269 and Glu 270 of tetanus toxin align to Glu 260 and Glu 261 of BoNT/A). Further, while the role of a tyrosine was anticipated^{1,22}, the structure indicates that it is the conserved Tyr 365 and not the conserved Tyr 232 which is within proximity to the zinc. While exact bond lengths and water molecules can not be confirmed at this resolution, the observed orientation of these residues support a model in which the His 222, His 226, and Glu 261 directly coordinate the zinc, and Glu 223 coordinates a water molecule as the fourth ligand. The Tyr 365 is ~5 Å from the zinc (OH--Zn) and is more likely to be involved in secondary bonding networks or interaction with substrate. Dali⁸, shows that the proteins with the most structural similarity to the catalytic domain are thermolysin (1hyt, Z=4.6) and leishmanolysin (1lml, Z=2.4), two other zinc proteases with the same conserved HEXXH sequence. The structural similarities are limited, however, to the helix containing the HEXXH sequence and a 4-

stranded β -sheet buttressing the helix. Beyond this overlap, the BoNT/A catalytic domain has different secondary structure elements and connectivities.

The catalytic domain of BoNT/A is highly specific for the C-terminus of SNAP-25 and appears to require a minimum of 16 substrate amino acids for cleavage²³. This large substrate size requirement is unusual for metalloproteases. The molecular recognition properties between the toxin and SNAP-25 and the dependence of recognition on a specific substrate secondary structure is presently being investigated^{24,25}. The channel (~12 Å x 15 Å x 35 Å) leading to the active site (Fig.4) appears capable of accommodating 16 or more residues with the Gln-Arg cleavage site of SNAP-25 able to insert into the zinc catalytic site. Additionally, the high pI of SNAP-25's C-terminal tail suggests that the negatively charged surface observed near the active site could be critical in the docking of substrate. Interestingly, the active site is most accessible in the absence of the translocation domain. This structure, in which the translocation domain shields the active site in the unreduced holotoxin, explains the fact that the catalytic activity in *in vitro* experiments is greatly enhanced by reduction of the disulfide. This observation of an occluded active site, along with the characterization of the amino acid environment, will almost certainly benefit ongoing inhibitor design.

Methods

Crystals were grown as described previously²⁶, but with a modified mother liquor of 150 mM magnesium acetate, 11% PEG 4000, and 100 mM tris-HCl pH 7. The crystals contain one monomer per asymmetric unit and are in spacegroup P3121 ($a = b = 170.5 \text{ \AA}$, $c = 161.1 \text{ \AA}$) with a solvent content of 70%. Derivatives were prepared by soaking crystals in: 1mM potassium tetrachloroaurate for 8-12 hrs, 1mM mercurous acetate for 6 hrs, 3mM methyl mercuric chloride for 6 hrs, 50mM samarium acetate for 12 hrs, or 0.5mM uranyl acetate for 6-10 hrs. Diffraction data for native and derivatized crystals were collected at 4 °C at SSRL, beamline 7-1 and beamline 9-1, at 1.08Å and 0.98Å, respectively. Crystals diffracted reasonably well for about 5 images using 1° oscillations before showing signs of radiation damage. Taking advantage of the high symmetry and the ability to translate bar shaped crystals allowed for complete data sets to be collected from a few crystals. All data were processed with DENZO and SCALEPACK²⁷, allowing for decreased resolution and increased mosaicity as the crystal decayed. The CCP4 suite of programs²⁸ was used for scaling the data sets and locating the heavy atom positions. Patterson maps were viewed with XCONTUR²⁹. MLPHARE²⁸ was used for heavy-atom position refinement and phase calculation. Phases were extended to 3.6 Å and improved by solvent flattening and histogram matching using the program DM³⁰. The model was built to 3.6Å resolution using the program O³¹, and then, as more data was collected, extended to 3.2 Å. Maps were improved with phase combination using SIGMAA³². Cycles of rebuilding, positional refinement, and simulated annealing using X-PLOR³³ were continued until convergence. Excellent electron density exists throughout the model and 99% of the amino acids were visible. Not surprisingly, the two ill-defined regions of the structure are the site of proteolytic cleavage between the two chains and in a surface loop immediately following His560 of the translocation domain.

Coordinates. Coordinates have been deposited in the Brookhaven Protein Data Bank under accession number 3bta.

Acknowledgments

We thank A. Cohen and M. Evenson for their help in the project, P. Kuhn and M. Soltis for their assistance at beamlines 7-1 and 9-1 at the Stanford Synchrotron Radiation Laboratory, R. Sweet at beamline X12C of the Brookhaven National Laboratory, T. Earnest at the Advanced Light Source, F. Lebeda for helpful discussions, and T. Umland for providing us with the tetanus toxin binding domain coordinates. Financial support for this research was provided by the U.S. Army Medical Research Institute of Infectious Diseases under contract DAMD17-93-C-3118.

Figure Legends

Fig. 1. Stereo diagram of the initial electron density. The map was calculated with MIR phases extended to 3.6 Å, improved by density modification, and contoured at 2.0σ . This region of the structure corresponds to the pair of α -helices in the translocation domain.

Fig. 2. Stereodiagram of the backbone trace for the BoNT/A model. The catalytic domain is colored in blue, the translocation domain in green, the N-terminal binding sub-domain in yellow and the C-terminal binding sub-domain in red. The catalytic zinc is depicted as a ball in gray. The "X" dictates the proteolytic site separating the two chains. The dashed line is the only loop region with ill-defined electron density. The lower view shows the model rotated ~90° out of the plane of the page relative to the top view and should better depict the translocation domain belt wrapping around the catalytic domain. The overall structure is 45 Å x 105 Å x 130 Å. Figure generated using MOLSCRIPT³⁴.

Fig 3. Stereo superposition of the BoNT/A binding domain (residues 873 to 1295) in red and the tetanus toxin binding domain (residues 874-1314) in yellow. The root mean square deviation is 1.5 Å for 363 C-alpha atoms. The major structural differences are in the C-terminal sub-domain loops.

Fig 4. Molecular surface of the catalytic domain colored by electrostatic potential (red=negative, blue=positive, white=uncharged). The active site is buried within the channel and appears largely negative. In the holotoxin, this pocket is partially blocked by the translocation domain belt. Figure generated using GRASP³⁵.

Fig 5. Stereo diagram of the catalytic domain active site. A σ_A -weighted $F_{\text{obs}} - F_{\text{calc}}$ omit map contoured at 2.6σ and centered around the zinc shows the amino acids (green carbon, red oxygen, and blue nitrogen bonds) thought to be critical for full catalytic activity. Figure generated using BOBSCRIPT.

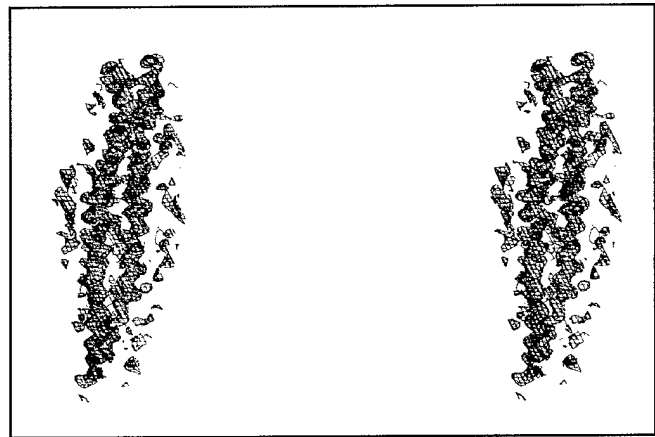


Figure 1

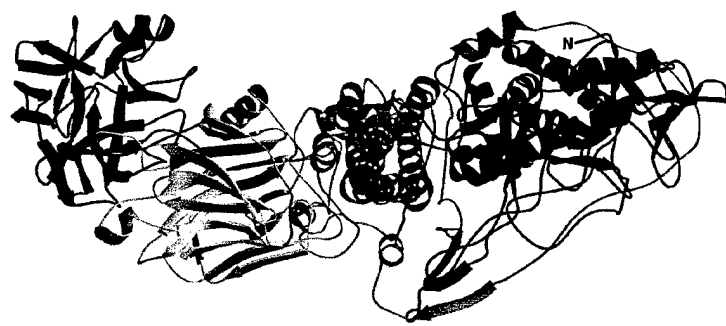
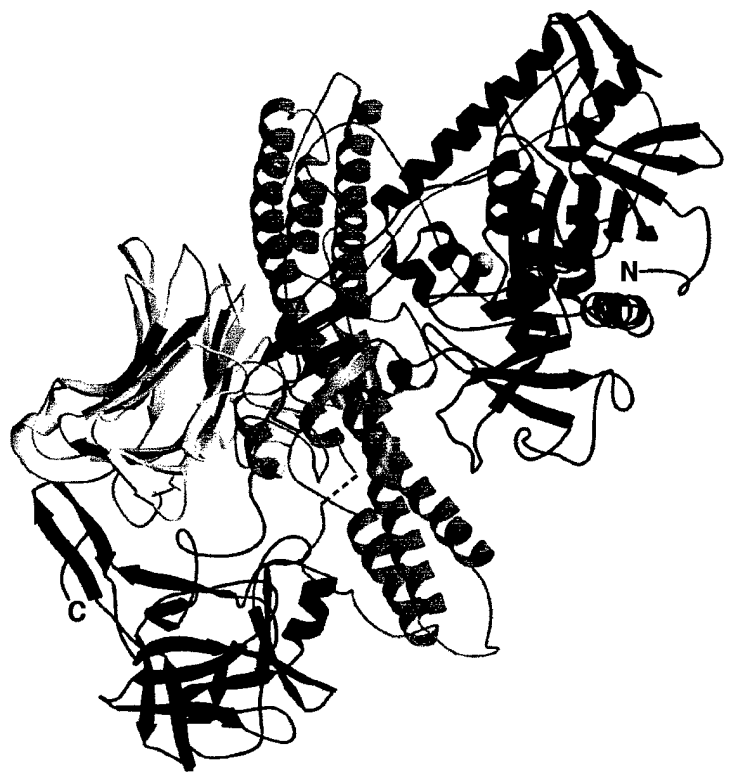


Figure 2



Figure 3

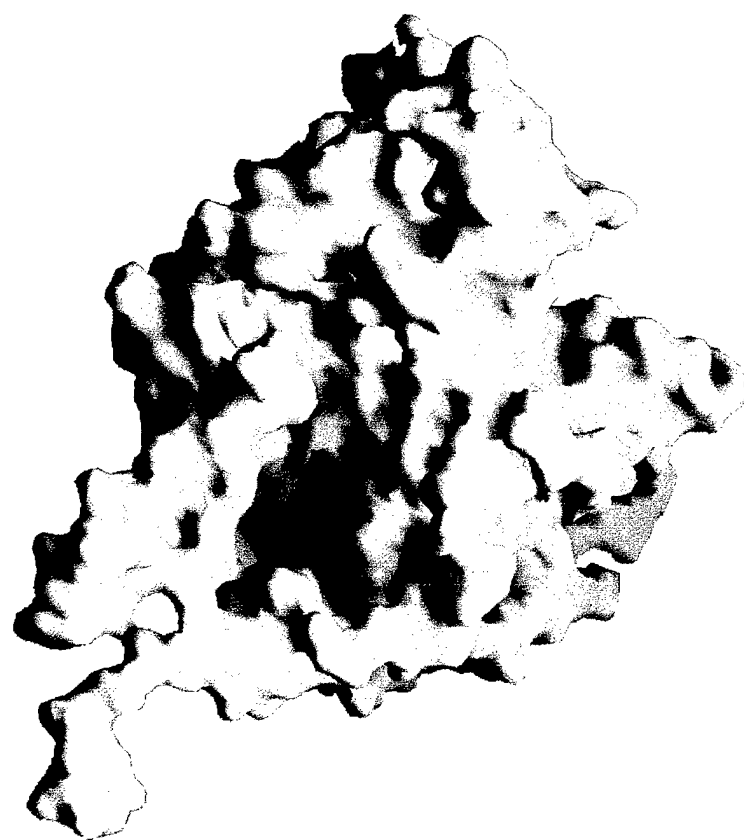


Figure 4

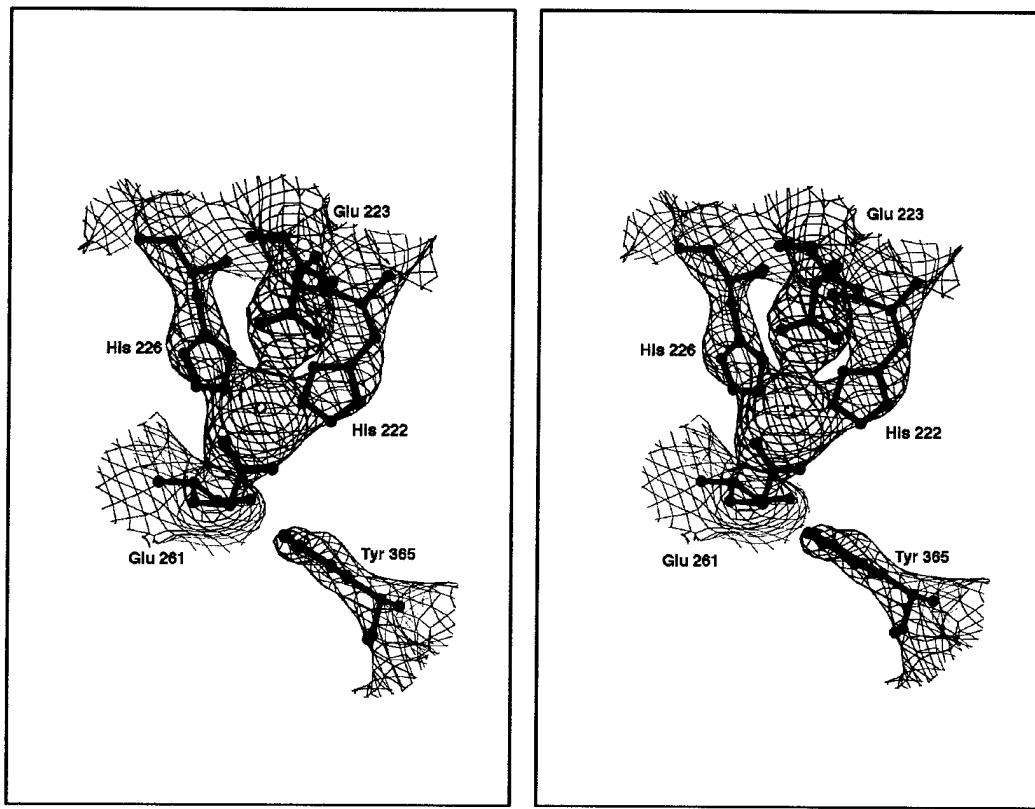


Figure 5

Table 1 Structure determination statistics**Diffraction data statistics**

Crystal	Resolution(Å)	Total obs.	Unique refl.	Completeness ¹ (%)	Rmerge ² (%)
Native	20-3.2	172,169	40,110	98.2(94.3)	11.1(48.3)
CH ₃ HgCl	15-4.5	87,457	15,830	97.2(96.0)	10.7(27.7)
Hg ₂ (Ac) ₂	15-4.2	86,260	19,650	97.8(94.3)	9.1(24.5)
SmAc	15-4.5	22,797	12,516	78.5(78.2)	7.6(17.4)
UAc	15-4.5	22,795	11,796	71.9(73.6)	7.8(22.5)
KAuCl ₄	15-6.0	19,894	6,080	93.7(95.5)	9.4(18.2)

Phasing statistics

Derivative	Number of sites ³	Isomorphous R- factor ⁴ (%)	Phasing power ⁵		RCullis ⁶	
			Cent.	Acent.	Cent.	Acent.
CH ₃ HgCl	6	21.7	1.03	1.64	0.68	0.65
Hg ₂ (Ac) ₂	6	21.0	0.96	1.36	0.76	0.76
SmAc	3	14.9	0.77	1.07	0.83	0.87
UAc	3	15.2	0.66	1.04	0.88	0.91
KAuCl ₄	1	15.2	0.63	1.03	0.88	0.88

FOM before solvent flattening 0.48
FOM after solvent flattening 0.74

Refinement statistics

R-factor/Free R	20.0/27.9
R.m.s.d. bond lengths	0.008 Å
R.m.s.d. bond angles	1.5 degrees

¹Numbers in parentheses indicate statistics for highest resolution shells.

²Rmerge = $S_h S_i |I_{hi} - \langle I_{hi} \rangle| / S_h S_i |I_{hi}|$, where h specifies unique indices, i indicates symmetry equivalent observations of h , and $\langle I_{hi} \rangle$ is the mean value.

³The mercury and gold derivatives shared overlapping sites. Similarly, the samarium and uranyl derivatives shared sites. However, the different occupancies yielded enough new phase information to improve the quality of the maps.

⁴The isomorphous R factor = $S_h ||F_{PH}|| - |F_p| / S_h |F_p|$, where $|F_{PH}|$ and $|F_p|$ are the measured structure factor amplitudes of the derivative and native structures.

⁵Phasing power is the mean value of the heavy atom structure factor amplitude divided by the residual lack of closure error.

⁶RCullis is the mean residual lack of closure error divided by the isomorphous difference.

References:

1. Montecucco, C. & Schiavo, G. Structure and function of tetanus and botulinum neurotoxins. *Quarterly Rev. Biophys.* **28**, 423-472 (1995).
2. Kriegstein, K. G., DasGupta, B. R., & Henschen, A. H. Covalent structure of botulinum neurotoxin type A: location of sulfhydryl groups, and disulfide bridges and identification of C-termini of light and heavy chains. *J. Prot. Chem.* **13**, 49-57 (1994).
3. Simpson, L. L. Kinetic studies on the interaction between botulinum toxin type A and the cholinergic neuromuscular junction. *J. Pharmacol. Exp. Ther.* **212**, 16-21 (1980).
4. Umland, T. C. et al. Structure of the receptor binding fragment Hc of tetanus neurotoxin. *Nature Struct. Biol.* **4**, 788-792 (1997).
5. Nishiki, T. et al.. The high-affinity binding of *Clostridium botulinum* type B neurotoxin to synaptotagmin II associated with gangliosides GT1b/GD1a. *Febs Letters* **378**, 253-257 (1996).
6. Montecucco, C. How do tetanus and botulinum toxins bind to neuronal membranes? *TIBS* **11**, 314-317 (1986).
7. Shapiro, R. E. et al. Identification of a ganglioside recognition domain of tetanus toxin using a novel ganglioside photoaffinity ligand. *J. Biol. Chem.* **272**, 30380-30386 (1997).
8. Holm, L. & Sander, C. The FSSP database of structurally aligned protein fold families. *Nucleic Acids Res.* **22**, 3600-3609 (1994).
9. Li, J. D., Carroll, J., & Ellar, D. J. Crystal structure of insecticidal delta-endotoxin from *Bacillus thuringiensis* at 2.5 Å resolution. *Nature* **353**, 815-821 (1991).
10. Choe, S. et al.. The crystal structure of diphtheria toxin. *Nature* **357**, 216-222 (1992).
11. Parker, M. W., Pattus, F., Tucker, A. D., & Tsernoglou, D. Structure of the membrane-pore-forming fragment of colicin A. *Nature* **337**, 93-96 (1989).
12. Allured, V. S., Collier, R. J., Carroll S. F., & McKay, D. B. Structure of exotoxin A of *Pseudomonas aeruginosa* at 3.0-Angstrom resolution. *Proc. Natl. Acad. Sci. U. S. A.* **83**, 1320-1324 (1986).

13. Muchmore, S. W. *et al.* X-ray and NMR structure of human Bcl-x_L, an inhibitor of programmed cell death. *Nature* **381**, 335-341 (1996).
14. Parker, M. W. & Pattus, F. Rendering a membrane protein soluble in water: a common packing motif in bacterial protein toxins. *TIBS* **18**, 391-395 (1993).
15. Wiener, M., Freymann, D., Ghosh, P., & Stroud, R. M. Crystal structure of colicin 1a. *Nature* **385**, 461-464 (1997).
16. Harrison, C. J., Hayer-Hartl, M., Di Liberto, M., Hartl, F., & Kuriyan, J. Crystal structure of the nucleotide exchange factor GrpE bound to the ATPase domain of the molecular chaperone DnaK. *Science* **276**, 431-435 (1997).
17. Oblatt-Montal, M., Yamazaki, M., Nelson, R., & Montal, M. Formation of ion channels in lipid bilayers by a peptide with the predicted transmembrane sequence of botulinum neurotoxin A. *Protein Science* **4**, 1490-1497 (1995).
18. Weissenhorn, W., Dessen, A., Harrison, S. C., Skehel, J. J., & Wiley, D. C. Atomic structure of the ectodomain from HIV-1 gp41. *Nature* **387**, 426-430 (1997).
19. Bullough, P. A., Hughson, F. M., Skehel, J. J., & Wiley, D. C. Structure of influenza haemagglutinin at the pH of membrane fusion. *Nature* **371**, 37-43 (1994).
20. Fass, D., Harrison, S. C., & Kim, P. S. Retrovirus envelope domain at 1.7 Å resolution. *Nature Struct. Biol.* **3**, 465-469 (1996).
21. Yamasaki, S. *et al.* Synaptobrevin/vesicle-associated membrane protein (VAMP) of *Aplysia californica*: structure and proteolysis by tetanus toxin and botulinal neurotoxins type D and F. *Proc. Natl. Acad. Sci. U. S. A.* **91**, 4688-4692 (1994).
22. Woody, M. & DasGupta, B. R. Effect of tetrinitromethane on the biological activities of botulinum neurotoxin types A, B, and E. *Mol Cell Biochem* **85**, 159-169 (1989).
23. Schmidt, J. J. & Bostian, K. A. Endoproteinase activity of type A botulinum neurotoxin: substrate requirements and activation by serum albumin. *J. Protein Chem.* **16**, 19-26 (1997).
24. Rossetto, O. *et al.* The metallo-proteinase activity of tetanus and botulinum neurotoxins. *J. Physiology (Paris)* **89**, 43-50 (1995).

25. Schmidt, J. J. & Bostian, K. A. Proteolysis of synthetic peptides by type A botulinum neurotoxin. *J. Protein Chem.* **14**, 703-708 (1995).
26. Stevens, R. C., Evenson, M. L., Tepp, W., & DasGupta, B. R. Crystallization and preliminary x-ray analysis of botulinum neurotoxin type A. *J. Mol. Biol.* **222**, 877-880 (1991).
27. Otwinowski, Z., in *Data Collection and Processing*, L. Sawyer, N. Isaacs, S. Bailey, Eds. (Science and Engineering Research Council, Warrington, UK, 1993), 56-62.
28. CCP4: *A Suite of Programs for Protein Crystallography* (SERC Daresbury Laboratory, Warrington WA4 4AD, UK, 1979).
29. McRee, D. E. A visual protein crystallographic software system for X11/Xview *J. Mol. Graphics* **10**, 44 (1992).
30. Cowtan, K. *Joint CCP4 ESF-EACBM Newslett. Protein Crystallog.* **31**, 34 (1994).
31. Jones, T. A., Zou, J.-Y, Cowan, S. W., & Kjelgaard, M. Improved methods for the building of protein models in electron density maps and the location of errors in these. *Acta Crystallogr. A* **47**, 110-119 (1991).
32. Read, R. J. Improved Fourier coefficients for maps using phases from partial structures with errors. *Acta Crystallogr.* **42**, 140-149 (1986).
33. Brunger, A.T., *X-PLOR v3.8*, Yale Univ. Press, New Haven, CT (1996).
34. Kraulis, P. J. MOLSCRIPT- a program to produce both detailed and schematic plots of protein structures. *J. Applied Crystallography* **24**, 946-950 (1991).
35. Nicholls, A., Sharp, K. A., & Honig, B. Protein folding and association: insights from the interfacial and thermodynamic properties of hydrocarbons. *Prot. Struct. Funct. Genet.* **11**, 281-296 (1991).
36. Lebeda, F.J., Olson, M.A. Secondary sturctural predictions for the clostridial neurotoxins. *Proteins* **20**, 293-300 (1994).